

Climate response to projected changes in short-lived species under an A1B scenario from 2000–2050 in the GISS climate model

Drew T. Shindell,^{1,2} Greg Faluvegi,^{1,2} Susanne E. Bauer,^{1,2} Dorothy M. Koch,^{1,2} Nadine Unger,³ Surabi Menon,⁴ Ron L. Miller,^{1,5} Gavin A. Schmidt,^{1,2} and David G. Streets⁶

Received 2 April 2007; revised 24 June 2007; accepted 7 August 2007; published 16 October 2007.

[1] We investigate the climate forcing from and response to projected changes in short-lived species and methane under an A1B scenario from 2000–2050 in the GISS climate model. We present a meta-analysis of new simulations of the full evolution of gas and aerosol species and other existing experiments with variations of the same model. The comparison highlights the importance of several physical processes in determining radiative forcing, especially the effect of climate change on stratosphere-troposphere exchange, heterogeneous sulfate-nitrate-dust chemistry, and changes in methane oxidation and natural emissions. However, the impact of these fairly uncertain physical effects is substantially less than the difference between alternative emission scenarios for all short-lived species. The net global mean annual average direct radiative forcing from the short-lived species is $.02 \text{ W/m}^2$ or less in our projections, as substantial positive ozone forcing is largely offset by negative aerosol direct forcing. Since aerosol reductions also lead to a reduced indirect effect, the global mean surface temperature warms by $\sim 0.07^\circ\text{C}$ by 2030 and $\sim 0.13^\circ\text{C}$ by 2050, adding 19% and 17%, respectively, to the warming induced by long-lived greenhouse gases. Regional direct forcings are large, up to 3.8 W/m^2 . The ensemble-mean climate response shows little regional correlation with the spatial pattern of the forcing, however, suggesting that oceanic and atmospheric mixing generally overwhelms the effect of even large localized forcings. Exceptions are the polar regions, where ozone and aerosols may induce substantial seasonal climate changes.

Citation: Shindell, D. T., G. Faluvegi, S. E. Bauer, D. M. Koch, N. Unger, S. Menon, R. L. Miller, G. A. Schmidt, and D. G. Streets (2007), Climate response to projected changes in short-lived species under an A1B scenario from 2000–2050 in the GISS climate model, *J. Geophys. Res.*, 112, D20103, doi:10.1029/2007JD008753.

1. Introduction

[2] While well-mixed greenhouse gases (WMGHGs) dominate both the radiative forcing since the preindustrial (PI) and the debate over global warming, short-lived species also play an important role. Hence it is important to better quantify their contribution to climate change. Additionally, mitigation of climate change via controls on short-lived species has several attractive features. Many of the short-lived species, ozone and the aerosols, are pollutants that cause substantial harm to humans, crops and natural eco-

systems. Thus controls on these radiatively active pollutants could provide health benefits in addition to climate change mitigation. In some cases, controls may be beneficial for health but detrimental for climate, a trade-off that needs to be considered carefully. The effects of controls could also be felt much more quickly than for WMGHGs, perhaps allowing substantial mitigation of radiative forcing over the next one to two decades, while more effective CO_2 emissions reduction strategies are developed (though prompt CO_2 emissions reductions using current technologies are nevertheless necessary to avoid many of the worst impacts of climate change [Hansen *et al.*, 2007a]).

[3] The short-lived species are inherently much more variable in space and time than the long-lived, however, making projection of their future concentrations extremely complex. Additionally, they are chemically reactive, and dependent upon one another, making it difficult to isolate the effects of a single species on climate [Shine *et al.*, 2005]. Furthermore, the atmospheric distribution is dependent upon a wide variety of sources and subsequent chemical transformations, many of which are fairly uncertain. In projects such as the Intergovernmental Panel on Climate Change (IPCC) Fourth Assessment Report (AR4) simula-

¹NASA Goddard Institute for Space Studies, New York, New York, USA.

²Center for Climate Systems Research, Columbia University, New York, New York, USA.

³Department of Atmospheric Sciences, University of Vermont, Burlington, Vermont, USA.

⁴Lawrence Berkeley Laboratory, Berkeley, California, USA.

⁵Department of Applied Physics and Applied Mathematics, Columbia University, New York, New York, USA.

⁶Argonne National Laboratory, Argonne, Illinois, USA.

Table 1. Simulations^a

Composition Runs	Emissions	Methane, ppmv	SSTs and Sea Ice
1995	EDGAR3.2 1995	1.75	1993–2002, obs.
2000*	IIASA 2000	1.75	1993–2002, obs.
2030*	2030 A1B	2.22	1993–2002, obs.
2050*	2050 A1B	2.40	1993–2002, obs.
2030_clim	2030 A1B	2.22	2026–2034, model
2050_clim	2050 A1B	2.40	2046–2054, model
2050_methane	2050 A1B	calculated	2046–2054, model
Climate runs	Time	Ensemble size	Ocean
Long-lived	2000–2050	3	[Russell <i>et al.</i> , 1995]
Long- and short-lived	2000–2050	3	[Russell <i>et al.</i> , 1995]

^aSST and sea ice fields are taken from the Hadley Center data set [Rayner *et al.*, 2003] for 1993–2002 observations, and from a prior GISS A1B coupled model simulation for the future using the same ocean and atmosphere models as used here [Hansen *et al.*, 2007a]. For methane, we give the global mean surface mixing ratio. * denotes composition simulation used to drive transient climate runs with short-lived species.

tions, while models generally used identical projections for the WMGHGs, the scenarios for short-lived species were quite varied. Those that did include short-lived species included only a subset of these, and did not isolate their impact from that of the WMGHGs.

[4] We attempt here to better characterize the effects of short-lived species and to provide input for the US Climate Change Science Program (CCSP) Synthesis and Assessment Product 3.2 “Climate Projections Based on Emission Scenarios for Long-lived and Short-lived Radiatively Active Gases and Aerosols”. We project the evolution of short-lived species following an A1B scenario, a mid-range projection from the Special Report on Emission Scenarios [Nakicenovic *et al.*, 2000], and the climate response to these species. For comparison, we also project the response to long-lived gases under this same scenario. These simulations can then be compared with similar studies undertaken at the NOAA Geophysical Fluid Dynamics Laboratory and the National Center for Atmospheric Research.

[5] Projections of climate change are made via a three-step process. First, projections of emissions of radiatively active species and their precursors are derived from Integrated Assessment Models (IAMs). Secondly, models are used to calculate the atmospheric abundance based on the projected emissions. For many species, especially WMGHGs, the IAMs themselves project future concentrations. For short-lived species, full 3D composition models are usually used. Finally, climate models simulate the climate response to the abundance changes. Our study includes both the second and third steps of this process, while the intercomparison with the other modeling groups will evaluate the effects of all three steps as projections from different IAMs were used by the different modeling centers. Additionally, we put our results in context by exploring the variations in composition resulting from: (1) uncertainties in some of the physical processes affecting the short-lived species, (2) different IAM projections of A1B emissions, and (3) the difference between A1B and other scenarios (note that the name A1 was used in the IAM runs, with the ‘B’ added later to denote ‘balanced’, referring to the balance between fossil fuel and renewable energy sources). This is accomplished primarily by comparison with prior GISS simulations with different model configurations or emissions.

[6] As one of our goals is to assess the role of those species whose reduction could have potential ancillary benefits in addition to their climate effects, and those with a response time that is rapid relative to the response time of CO₂ (centuries), we also explore the potential future behavior of methane in some detail. Methane, unlike the other WMGHGs, is chemically reactive in the troposphere and stratosphere and thus has a lifetime of only about a decade. It is also a valuable commodity (the main component of natural gas), providing ancillary benefits if it is captured rather than released to the atmosphere [West *et al.*, 2006]. Finally, it plays an important role in tropospheric ozone chemistry and thus the tropospheric oxidation capacity, and hence is intimately connected to the short-lived species [Fiore *et al.*, 2002; Shindell *et al.*, 2005]. Following conventional definitions of WMGHGs, we include methane among the long-lived rather than the short-lived species, but explore the potential for methane to deviate substantially from the IAM projections due to interactions of natural emissions with climate change and to the effects of tropospheric chemical changes on methane loss rates.

2. Experimental Setup

[7] The simulations described here consist of several parts. First, emission inventories for future times were constructed. Second, simulations of short-lived species were performed using the GISS chemistry-aerosol model for present-day (PD) and future time periods. Finally, the resulting concentration fields were used to drive transient climate simulations to isolate the effect of short-lived species in the future. Here we describe the data and models used for each step.

2.1. Emissions and Abundances

[8] Inventories of emissions for short-lived species and their precursors were prepared for 2000, 2030, and 2050 for use in the composition runs (Table 1). The 2000 simulation uses the 2000 emission inventory of the International Institute for Applied Systems Analysis (IIASA), except for biomass burning which is taken from the Global Fire Emission Database (GFED) averaged over 1997–2002 [Van der Werf *et al.*, 2003] (Table 2) with emission factors from [Andreae and Merlet, 2001] for aerosols. The IIASA

Table 2. Emissions of Short-Lived Species and Their Precursors (Tg/yr)^a

	1995 EDGAR	2000 IIASA	2030 A1B	2050 A1B
NO _x	44.6	48.4	64.8 (34%)	75.2 (55%)
CO	829	1002	1002 (0%)	1153 (15%)
Alkenes	53.4	53.8	49.3 (−8%)	66.1 (23%)
Paraffins	107.7	103.5	173.3 (67%)	154.6 (49%)
Isoprene	356	356	356	356
SO ₂	83.5	65.1	101.1 (56%)	82.2 (27%)
SO ₄	2.1	1.6	2.5 (58%)	2.1 (33%)
BC	—	8.7	6.8 (−22%)	5.9 (−32%)
OC	—	71.1	56.6 (−20%)	57.5 (−19%)
NH ₃	68.9	68.5	72.2 (5%)	74.1 (8%)

^aValues are the sum of natural emissions plus the anthropogenic emissions from the given inventory/scenario. Emissions are in Tg N/yr for NO_x, Tg C/yr for lumped alkenes and paraffins, Tg S/yr for sulfur-containing species, and Tg/yr of the species for others. Changes in the total emission for each species are given in parenthesis in percent relative to 2000. Dust emissions are constant at 1580 Tg/yr.

inventory is based on the 1995 EDGAR3.2 inventory, extrapolated to 2000 using national and sector economic development data [Dentener *et al.*, 2005]. This is the same inventory as used in several recent multimodel intercomparisons of future tropospheric chemistry [Dentener *et al.*, 2006; Shindell *et al.*, 2006b; Stevenson *et al.*, 2006]. Lightning NO_x emissions are calculated internally in the GCM, and other natural sources are prescribed according to conventional estimates (Table 2).

[9] Future simulations are driven by projected emissions changes following an A1B scenario. Many IAM groups used the A1 socio-economic storyline to drive their models, providing a range of results to the IPCC Special Report on Emission Scenarios (SRES) [Nakicenovic *et al.*, 2000]. The IMAGE model [IMAGE Team, 2001] provided relatively complete documentation of their calculations, and included explicit energy and fuel usage trends over 17 different regions. Other IAMs provided results for as few as 4 regions. The level of detail in the IMAGE results allowed [Streets *et al.*, 2004] to estimate consistent regional growth factors for all the relevant precursor emissions. This included carbonaceous aerosols, which were not included in the original IAMs, for which the emissions projections created in [Streets *et al.*, 2004] included expected changes in technology. We point out that the IMAGE model results submitted to the SRES were subsequently revised, and we use the finalized projections throughout this study.

[10] We then apply these projections to the EDGAR3.2 1995 inventory to derive the full spatial distribution of emissions for each source. Thus both the IIASA 2000 and the future A1B emissions are based on the same EDGAR3.2 1995 inventory. The resulting future emissions do not necessarily match the global total emissions values reported by the IMAGE model to the SRES, but generally follow their results. The most notable exception is the projection for SO_x emissions, which were substantially reduced in the revisions subsequent to the SRES (Figure 1). We also take projections of biomass burning changes (which are applied to all emitted species) from [Streets *et al.*, 2004]. Note that emissions for a given species depend upon projections for many individual sources, and these may have different

emissions factors for each species. Hence black carbon (BC), with greater emissions from fossil fuel burning, declines more rapidly than organic carbon (OC), whose emissions depend more on vegetation burning (Figure 1). The one species whose emissions were not based on the IMAGE A1 projections is NH₃. Projections instead come from IIASA as the A1B emissions were not yet available at the time the simulations were performed. The effects of these differences are discussed further below, however.

[11] The IMAGE model A1 projections are somewhat different from the results of another IAM, the AIM model (Figure 1). These latter emissions projections are widely used, as the SRES referred to them as a ‘marker’ scenario. The SRES defines this as “a scenario that was originally posted on the SRES web site to represent a given scenario family”. However, they also note that their ‘marker’ scenarios do not represent the average, best, or median results, and that all IAM results should be treated equally. Thus we

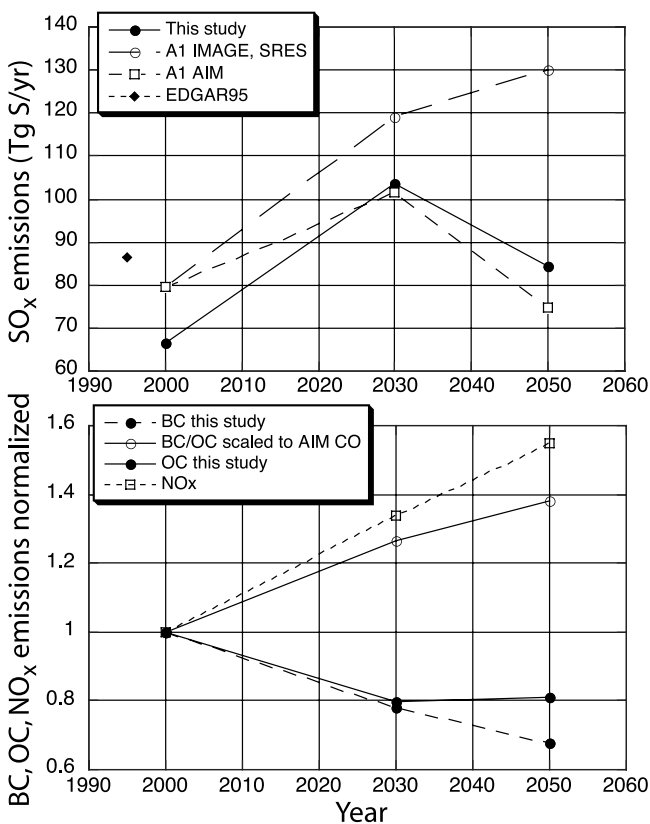


Figure 1. Emissions trends for SO_x, NO_x, and carbonaceous aerosols. Trends for SO_x (top) are shown for this study (using the IIASA inventory for 2000 and A1 IMAGE model revised 2001 output), for the A1 AIM model, and for the original A1 IMAGE model output from the SRES. Emissions in the EDGAR 1995 inventory are also shown for comparison. All SO_x emissions include 10.7 Tg S/yr from volcanoes. Normalized carbonaceous aerosol and NO_x emissions (bottom) are shown for this study based on [Streets *et al.*, 2004] and values for BC/OC are also given using the TAR suggested scaling according to CO based on the CO projections from the A1 AIM ‘marker’ scenario.

believe the advantages of the IMAGE model's documentation and regional detail make it a good choice. We compare with the AIM emissions projections to put these results in context, however. As emissions of several species show increases from the present through 2030 followed by decreases, we concentrate on the present (2000), the inflection point (2030), and the end of our chosen period (2050).

[12] For consistency with the GISS AR4 A1B climate simulations [Hansen *et al.*, 2007a], the long-lived gases CO₂, N₂O, and fluorocarbons are prescribed at A1B concentrations from the AIM model. These are qualitatively similar to those from the IMAGE model, but increase ~20% more slowly. Methane was also prescribed following the AIM model, however a separate simulation exploring the methane abundance calculated with our model was also run. We note that while the A1B projections assume a substantial increase in atmospheric methane in the future, the growth rate of methane has in fact decreased markedly since the early 1990s and leveled off since ~1999 [Dlugokencky *et al.*, 2003]. Hence the projections may overestimate future atmospheric concentrations. However, there are indications that the growth rate decrease was primarily due to reduced anthropogenic emissions, and that these have begun increasing again since 1999 (though masked by a coincident decrease in natural methane emissions) [Bousquet *et al.*, 2006]. This suggests that atmospheric methane may increase substantially in the future, as the IAMs assumed.

2.2. Composition Model

[13] The components of the GISS composition model have been described in detail in several recent papers. Photochemistry extends seamlessly from the surface to the mesosphere, and hence responds to changes in surface emissions of ozone precursors, the abundance of ozone-depleting substances in the stratosphere, and to GHGs (via temperature and chemistry) [Shindell *et al.*, 2006a]. Aerosols include sulfate, carbonaceous aerosols, and sea salt [Koch *et al.*, 2006; Koch *et al.*, 2007a], nitrate aerosols [Bauer *et al.*, 2006], and mineral dust [Miller *et al.*, 2006a]. Dust is segregated into 4 size bins, while only total mass is simulated for the other aerosols. Most importantly, these components interact with one another, with linkages including oxidants affecting sulfate, gas-phase nitrogen species affecting nitrate, sulfate affecting nitrogen heterogeneous chemistry via reaction of N₂O₅ to HNO₃, thermodynamic ammonium nitrate formation being affected by sulfate, sea salt and mineral dust [Metzger *et al.*, 2006], and sulfate and nitrate being absorbed onto mineral dust surfaces (i.e., the aerosols are internally mixed as coatings form on dust surfaces [Bauer *et al.*, 2006]). Several prior studies have examined projected composition changes leaving out some of these linkages. Comparison with these studies thus allows us to quantify the importance of some individual processes. The simulations described here were run using a 23-layer, 4 by 5 degree horizontal resolution version of the ModelE GCM [Schmidt *et al.*, 2006].

[14] Present-day results in the model are generally similar to those in the underlying chemistry and aerosol models documented previously, with a few exceptions. The model used here does not include the enhanced convective scavenging of insoluble species prescribed in [Koch *et al.*, 2007a]. Therefore our carbonaceous aerosol burden, espe-

cially in the free troposphere, is nearly double that of [Koch *et al.*, 2007a]. Agreement with the limited available observations is comparable between the two simulations (a positive bias replaces a negative bias). Sulfate in this model is biased low due to a rate coefficient error discovered after the simulations were completed that reduced oxidation of SO₂ to SO₄. Comparison with earlier PD simulations with a similar coupling between chemistry, sulfate and nitrate indicate that the error biased the gas-phase sulfate low by ~20%, but had virtually no effect on the sulfate absorbed onto dust. We note that the uncertainty associated with heterogeneous removal of sulfate onto dust is considerably larger than the effect of the erroneous rate coefficient, and that we were able to compensate for the bias in the climate simulations (see below). Other species compare reasonably well with available observations, as shown in the papers mentioned previously.

[15] The model contains a full methane cycle, including spatially and seasonally varying surface emissions from multiple sources, atmospheric oxidation, and loss to soils [Shindell *et al.*, 2003]. Emissions from wetlands can vary as a function of climate [Shindell *et al.*, 2004]. Given projections of anthropogenic methane emissions, the model can thus calculate the resulting atmospheric abundance. In the current study, we perform runs using prescribed methane abundances and also a run using results from the full methane cycle calculation. This run complements the other time slices performed (Table 1).

2.3. Climate Model

[16] The climate simulations, like the composition simulations, were performed using GISS ModelE [Schmidt *et al.*, 2006]. We use a 20-layer version of the atmospheric model with 4 by 5 degree horizontal resolution coupled to a dynamic ocean, as in the GISS-ER IPCC AR4 simulations [Hansen *et al.*, 2007a]. This model has been extensively evaluated against observations [Schmidt *et al.*, 2006], and has a climate sensitivity similar to that of mainstream GCMs (2.6°C for doubled CO₂) and in accord with values inferred from paleoclimate data. It captures the variability associated with the large-scale annular modes reasonably well, and roughly in accord with other GCMs [Miller *et al.*, 2006b]. The model differs from the 23-layer model used in the composition modeling only in the stratosphere, which has more layers and a gravity-wave drag parameterization in the 23-layer version. These features are important for the modeling of ozone, but less so for the climate simulations.

[17] The modeled radiatively active species influence the climate in the GCM. Ozone and aerosols can affect both the short and long wavelength radiation fluxes. Water uptake on aerosol surfaces influences the aerosol effective radius, refractive index and extinction efficiency as a function of wavelength and the local relative humidity [Koch *et al.*, 2007a], which in turn affects the GCM's radiation field. To attempt to provide more realistic aerosol forcing in prior GISS simulations, carbonaceous aerosols generated with an older version of the composition model were scaled up by factors of 2.5 for OC and 1.9 for BC [Hansen *et al.*, 2007a]. As the carbonaceous aerosol fields in the new composition model are in reasonable agreement with observations, and in fact slightly overestimated, this scaling was removed in the current runs. To compensate for the ~20% low bias in

sulfate, we scaled that aerosol by 1.2 for the transient climate simulations.

[18] The model also includes a parameterization for the aerosol indirect effect [Menon *et al.*, 2002], which we use in a manner consistent with GISS AR4 20th century simulations. This includes cloud cover changes following an empirical logarithmic dependence on the number concentration of soluble aerosols, where the latter is determined from the aerosol masses based on densities and solubilities prescribed for each species as in [Hansen *et al.*, 2005]. Carbonaceous aerosols become soluble after aging in the model, so the aerosol indirect effect depends upon BC, OC, sulfate and nitrate. We use only cloud cover changes (the 2nd indirect effect), with empirical coefficients chosen to give roughly -1 W/m^2 forcing from the PI to the PD, a value chosen to match diurnal temperature and satellite polarization measurements, as described in [Hansen *et al.*, 2005]. We note that this forcing is roughly twice the value used in many other model studies [Penner *et al.*, 2006]. The aerosol indirect effect in the model takes place from the surface through the layer centered at 630 hPa, as we only let aerosols affect liquid-phase stratus clouds. The model includes the influence on albedo of the deposition of BC on snow, but the BC deposition is not yet coupled with the chemistry-aerosol modules and hence is fixed at the PD amount.

2.4. Simulations

[19] The composition model is embedded within the GISS climate model, allowing an altered climate to influence the composition calculation. While the simulations of the climate response to changes in the short-lived species could thus have been performed with online composition, this is in practice too computationally expensive. Hence the composition simulations are run for only 2 years, with the output from the last year alone used in the subsequent transient climate runs. Comparison of the first and second years reveals that interannual variability is actually rather small for monthly averages, so that while longer simulations would have been preferable, we believe the results are likely to be representative. We note, however, that use of offline composition fields may influence the results. For example, if the tropopause moves upwards relative to its offline location, stratospheric ozone values could be used in the uppermost troposphere. Issues of offline versus online coupling should be studied further.

[20] Composition simulations are performed for 2000, 2030, and 2050 and were run both with and without projected surface climate changes. The latter are imposed via prescribed sea surface temperatures (SSTs) and sea ice coverage (Table 1). Both sets of runs used projected WMGHGs, so even the runs without ocean surface changes are not fully fixed climates, but include land and atmospheric temperature changes (the relatively fast climate responses). To better characterize interannual variability, and to test the robustness of the climate induced changes, the two 2050 simulations were extended to 4 years. Additional runs were performed using EDGAR 1995 emissions, to facilitate comparison with prior runs, and with calculated methane at 2050, as noted previously (Table 1). We note that the composition simulations without prescribed surface climate changes were the ones used to drive the transient

climate simulations, for consistency with the other CCSP modeling groups. As natural mineral dust and sea-salt emissions could therefore not respond to climate change, these species were not passed from the composition model for the climate runs, which instead kept those fixed through time.

[21] The climate simulations consist of two sets of transient 3-member ensemble climate runs from 2003–2050 (the runs began at 2003 instead of 2000 for technical reasons). One set includes the evolution of both short- and long-lived species following the A1B scenario, using short-lived species concentrations from the model calculations described above with values linearly interpolated between the timeslices. The other includes time-varying concentrations only for the long-lived species, while the short-lived species are fixed at their 2000 amounts. We note that the latter simulations are similar to those performed for the AR4, but not identical. The difference arises because the AR4 runs used PD concentrations of short-lived species from earlier versions of the composition models. The change resulting from the new distributions induces a small difference in the planetary energy balance at 2000, necessitating the otherwise similar runs with fixed short-lived concentrations performed here.

3. Composition Projections

3.1. Changes at 2030 and 2050 and Their Radiative Forcing

[22] Future burdens of the radiatively active short-lived species are given in Table 3 along with the percentage burden change normalized to the percentage total emission change of the primary precursor. Ozone changes generally follow the emissions projections for NO_x quite closely, at least for the global mean. These will have also been affected by the increases in VOC and CO emissions and methane abundance, of course. Sulfate appears to have a fairly linear response as well over the small range sampled here, with a burden change $\sim 60\%$ of the sulfur dioxide emissions perturbation. The carbonaceous aerosol burdens show more non-linearity, especially organic carbon, which has a rather different response in 2050 than in 2030. As we have only three time-slices, this clearly requires further study. The global mean behavior of the different short-lived species varies markedly, with ozone and nitrate increasing and BC and OC decreasing throughout 2000 to 2050, while sulfate increases from 2000 to 2030 but decreases thereafter, returning to roughly its 2000 value in 2050.

[23] Aerosol optical depths (AOD) by species are given in Table 4. With much of the sulfate burden absorbed onto dust [Bauer and Koch, 2005], the dominant species are dust and sea salt. This is true in both the global and hemispheric averages, and sea salt is the larger of the two, especially in the SH. For comparison with observations, we compute clear-sky AOD as well as all-sky. For computational efficiency, each grid-box is assigned to be either cloud-free or fully cloud-covered for the radiative transfer calculation in the GISS GCM based on a combination of random chance and the fractional cloud cover in the box. We use these cloud-free radiative transfer calculations for the clear-sky AOD. Hence our calculation is geographically weighted toward less cloudy areas, as are the clear-sky satellite AOD

Table 3. Global Burdens of Short-Lived Species (Tg Species, Tg C for BC/OC) and Scaling With Emissions^a

	1995	2000	2030	2030 clim	2050	2050 clim	2030 vs 2000 Δ burden/ Δ emission	2050 vs 2000 Δ burden/ Δ emission
O ₃	333	344	452	447 (−1%)	521	555 (7%)	.93	.94
SO ₄ burden	.94	.82	.99	1.02 (3%)	.93	.95 (2%)		
SO ₄ on dust	.77	.67	1.00	.97 (−3%)	.82	.86 (6%)		
SO ₄ total	1.71	1.50	2.00	1.98 (−1%)	1.76	1.81 (3%)	.59	.61
BC	.249	.249	.187	.185 (−1%)	.147	.149 (1%)	1.22	1.32
OC	1.62	1.62	1.30	1.30 (0%)	1.24	1.25 (1%)	.97	1.21
NO ₃ gas	.36	.37	.37	.36 (−3%)	.42	.36 (−14%)	-	1.69
NO ₃ on dust	1.88	1.92	2.39	2.20 (−10%)	2.77	2.52 (−13%)		
NO ₃ total	2.24	2.29	2.76	2.56 (−9%)	3.19	2.88 (−10%)		

^aRatios of the change in the burden to the change in emissions are calculated based on the fractional changes in each, using the total emissions of the species for BC and OC, and otherwise of the primary precursor (SO₂ for SO₄, NH₃ for NO₃, and NO_x for O₃). Dust burden is constant at 35 Tg. The ozone burden is for the troposphere only. Changes due to climate at 2030 and 2050 are shown in parentheses as percent of the 2000 value.

data. The total PD global mean clear-sky optical depth is 0.12, slightly lower than the values of 0.135 derived from ground-based AERONET observations or the satellite composite value of 0.151 [Kinne *et al.*, 2006]. Neither of the observation-based data sets are fully global, however.

[24] Our results are broadly consistent with other models, which now produce total AODs in the range of 0.10–0.15 [Kinne *et al.*, 2006]. The relative importance of individual aerosol species varies dramatically among the models however. While the contribution from BC is always small, some models have sea salt and dust together contributing more than 2/3 of the AOD, while others have OC and sulfate contributing the majority of the AOD. In our model, the dominance of sea salt and dust, which have largely natural sources and were not varied in these simulations, leads to a relatively small impact from changes to anthropogenic sulfate and carbonaceous aerosols. Hence the forcings in our model change little with time, especially in the SH (Table 4).

[25] Ozone changes were simulated throughout the troposphere and stratosphere (Figure 2). Ozone responded to both the changes in emissions of short-lived precursor species, whose direct influence is primarily in the troposphere, and to changes in the abundance of long-lived species (CO₂, N₂O, CH₄, and CFCs) that affect both stratospheric composition directly and indirectly by altering local temperatures. Ozone increases nearly everywhere in the future, with especially large changes in the vicinity of the mid- to high-latitude tropopause owing to the reduction of halogens. The halogen reduction, combined with enhanced greenhouse gas cooling, also leads to a substantial increase in the upper stratosphere. The projected stratospheric ozone recovery extends down into the troposphere, especially in the SH, as there is a substantial downward flux of extratropical ozone from the stratosphere to the troposphere (the model's PD stratosphere-troposphere exchange (STE) is 504 Tg/yr, in good agreement with values inferred from observations [Gettelman *et al.*, 1997]). This result emphasizes the importance of full-atmosphere chemistry simulations.

[26] Our results are consistent with observations indicating that stratospheric ozone depletion has likewise influenced ozone down to the surface [Oltmans *et al.*, 1998]. When 2050 climate change is included (via SSTs), enhancement of the Brewer-Dobson circulation leads to an increase

in the flux of stratospheric ozone into the polar lower stratosphere and into the troposphere (2050 STE increases from 893 to 1027 Tg/yr based on the average of the 4 years of the runs), especially in the NH (Figure 2), as seen in our earlier studies [Shindell *et al.*, 2006a]. Other modeling groups have also found substantial increases in STE under projections of future climate alone [Collins *et al.*, 2003] or of future climate and composition [Sudo *et al.*, 2003; Zeng and Pyle, 2003], and similarly show a substantial impact on the troposphere.

[27] SST changes have little direct effect on most of the stratosphere, where temperature changes are largely due to local composition changes. They do enhance the overturning circulation, as noted previously, leading to increased ozone at high latitudes. They also cause a small decrease in ozone in the tropical stratosphere as they lead to an

Table 4. Aerosol Optical Depth (550 nm Extinction)^a

Region	Aerosol Type	2000	2030	2050	2000 Clear-Sky
Global	BC	.0045	.0034	.0028	.0046
	Sulfate	.0250	.0312	.0278	.0127
	OC	.0166	.0135	.0130	.0170
	Nitrate	.0054	.0057	.0060	.0034
	Dust	.0372	.0372	.0372	.0375
	Sea-salt	.1065	.1065	.1065	.0418
	Total	.1952	.1975	.1933	.1171
NH	BC	.0062	.0043	.0032	.0063
	Sulfate	.0352	.0449	.0388	.0169
	OC	.0176	.0134	.0121	.0182
	Nitrate	.0091	.0098	.0103	.0055
	Dust	.0600	.0600	.0600	.0605
	Sea-salt	.0630	.0630	.0630	.0225
	Total	.1910	.1954	.1875	.1300
SH	BC	.0029	.0026	.0023	.0030
	Sulfate	.0148	.0175	.0170	.0085
	OC	.0155	.0135	.0139	.0158
	Nitrate	.0017	.0015	.0018	.0013
	Dust	.0144	.0144	.0144	.0144
	Sea-salt	.1502	.1502	.1502	.0611
	Total	.1995	.1998	.1996	.1042
Clear-sky, global	Total	.1171	.1178	.1145	
Clear-sky NH	Total	.1300	.1321	.1263	
Clear-sky SH	Total	.1042	.1034	.1028	

^aValues are all-sky except where noted. These values include the scaling of 1.2 applied to sulfate in the transient climate simulations, though given the small value for sulfate this has little effect on total optical depth.

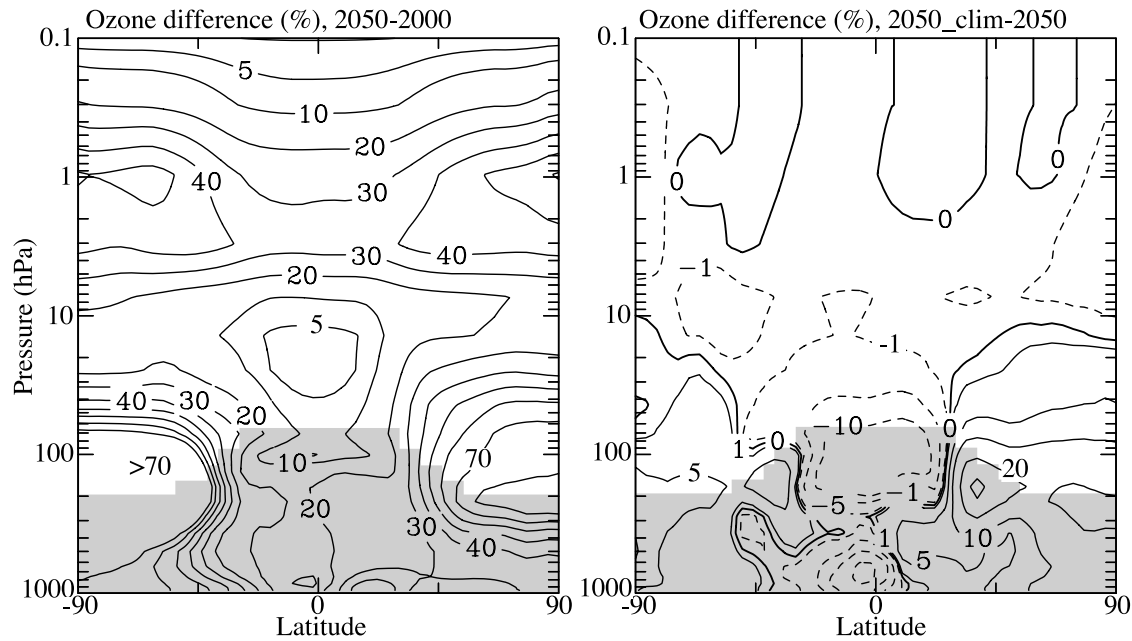


Figure 2. Zonal mean annual average ozone change (%) between 2050 and 2000 due to emissions (left) and the change at 2050 due to climate (via SSTs, 2050_clim-2050) (right). Shading indicates the area below the annual mean zonally averaged tropopause (PD climate location).

enhanced influx of water due to a warming of the tropical tropopause. Warmer SSTs enhance water in the troposphere substantially, leading to ozone decreases, especially in the tropics, by augmenting odd oxygen loss via reaction of singlet-D atomic oxygen with water.

[28] The largest single radiative forcing at 2030 and 2050 comes from these ozone changes (Table 5). Our RF of 0.13 W/m^2 at 2030 is roughly twice the $.06 \text{ W/m}^2$ multimodel mean RF at 2030 due to tropospheric ozone alone and based on a somewhat different emissions projec-

Table 5. Global Mean Annual Average Radiative Forcing (W/m^2)^a

Forcings relative to 2000 in this study								
	2030	2030_clim	2050	2050_clim				
Ozone	.13	.14	.19 (.20)	.25 (.26)				
Sulfate	−.10	−.11	−.06 (−.06)	−.07 (−.07)				
Nitrate	−.004	−.001	−.015 (−.018)	.004 (.004)				
Black	−.09	−.09	−.16 (−.16)	−.16 (−.16)				
Carbon								
Organic	.06	.06	.06 (.05)	.06 (.06)				
Carbon								
Net	.00	.00	.02 (.01)	.09 (.10)				
Forcings relative to 1995 in this and prior studies								
	2030 This study	2030_clim This study	2030 Unger et al	2030 Koch et al	2030 Bauer et al	2050 This study	2050_clim This study	2050 Koch et al
Ozone	.18	.19	.19			.23	.30	
Sulfate	−.05	−.06	−.24	−.14		−.02	−.03	−.05
Nitrate	−.005	−.002			−.03	−.016	.005	
Black	−.09	−.09		−.04		−.16	−.16	−.07
Carbon								
Organic	.06	.06		.02		.06	.06	.01
Carbon								
Net	.09	.10				.09	.18	

^aAll values are instantaneous values at the tropopause (except for those of [Koch et al., 2007a] which are at the top of the atmosphere, but this should have minimal effect given that these are tropospheric perturbations). Values are from the second year of two-year runs (numbers in parentheses indicate averages over last 3 years of 2050 runs extended to four years). Values for sulfate include the 1.2 scaling used in the transient climate simulations. Results from [Unger et al., 2006] do not include climate change (for comparison with Koch et al results). All values are direct forcing only (no aerosol indirect effects).

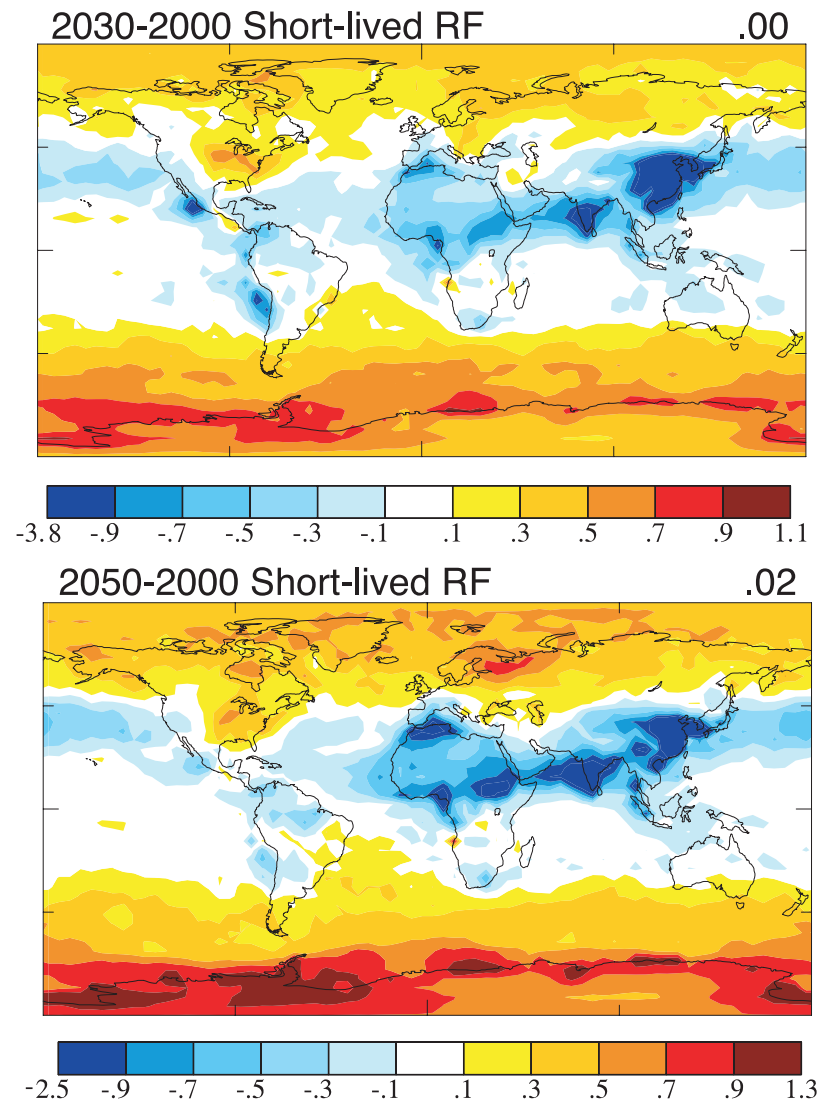


Figure 3. Total annual average instantaneous tropopause radiative forcing (W/m^2) from all short-lived species at 2030 (top) and 2050 (bottom) relative to 2000 in the composition simulations without climate change that were used to drive the transient climate experiments. The value at the upper right is the global mean.

tion (IIASA ‘current legislation’ instead of A1B) [Stevenson *et al.*, 2006]. This seems reasonable given that we include the influence of stratospheric ozone recovery. Stratospheric ozone depletion contributed -0.06 W/m^2 from the PI to PD in our earlier studies [Shindell *et al.*, 2006a], so that its partial recovery by 2030 should contribute a small positive forcing. Another multimodel comparison that included limited representation of the stratosphere found a RF at 2100 due to stratospheric ozone increases driven by both increasing tropospheric pollution and reductions in ozone depleting substances in the stratosphere of $0.15\text{--}0.17 \text{ W/m}^2$ [Gauss *et al.*, 2003]. This value exceeds our stratospheric ozone RF, but it is farther in the future and based on the very large increases in tropospheric pollutants. Hence our ozone RF seems broadly in line with other studies.

[29] The net direct aerosol forcing in 2030 exactly offsets the positive forcing from ozone. At 2050, the situation is broadly similar, with net direct aerosol forcing (-0.17 W/m^2) offsetting roughly 90% of the positive forcing from ozone.

However, the relative importance of the aerosols has shifted. While sulfate forcing was most important in 2030, as the carbonaceous aerosols largely offset one another, the reduction in black carbon dominates over all the other aerosol changes in 2050.

[30] The spatial structure of the net direct radiative forcing is quite heterogeneous (Figure 3). Values are generally positive at high latitudes and near zero over much of the tropical and subtropical oceans. Positive values also occur over most of the midlatitudes in the SH, and in some parts of the NH such as North America. There are strong negative forcings over much of the NH tropical and subtropical continental area in the Eastern Hemisphere.

[31] The causes of these spatial patterns are readily determined by examination of the forcing from individual species (Figure 4). Ozone increases are greatest at high-latitudes, where recovery from halogen-induced depletion in the lower stratosphere plays the largest role. The increases themselves extend into the troposphere due to transport,

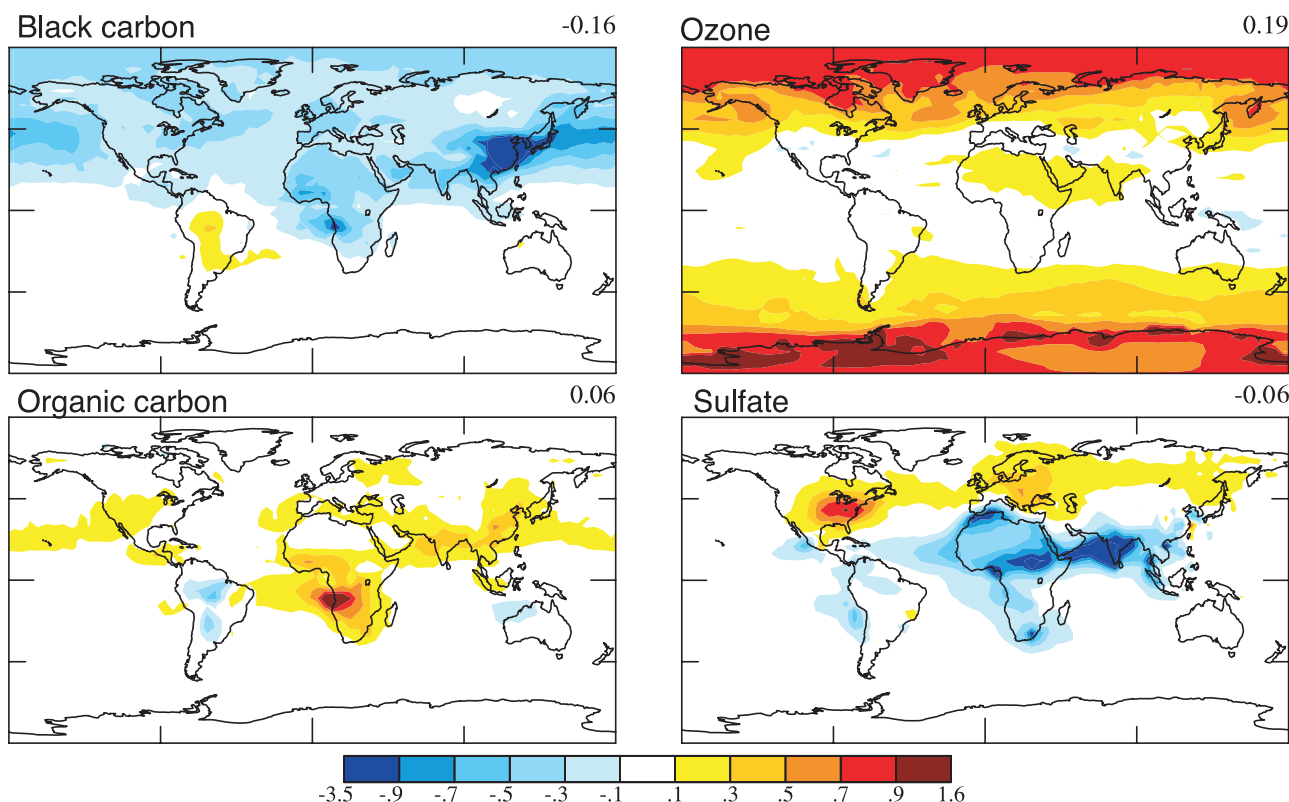


Figure 4. Annual average instantaneous tropopause radiative forcing (W/m^2) from individual short-lived species at 2050 relative to 2000 in the simulations without climate change. Value in the upper right corner gives the global mean. Radiative forcing from nitrate does not show any areas with forcing greater than 0.1 W/m^2 or less than -0.1 W/m^2 (the white color bar). Aerosol values are direct forcing only.

leading to maximum increases centered on the tropopause (Figure 2), precisely where their RF is largest. This leads to the sizable positive middle and high latitude forcings. Tropical ozone forcing is comparatively small, despite substantial increases in projected tropical precursor emissions, due to increases in overhead ozone. At high altitudes, where these increases are largest (Figure 2), they have a cooling effect, and hence offset some of the RF due to increases at lower altitudes. Additionally, the increase in the stratospheric ozone column could affect tropical upwelling by altering vertical stability and could reduce photochemical ozone production in the troposphere by limiting UV flux. This result is consistent with observations, which show anticorrelations between tropical stratospheric and tropospheric ozone [Ziemke and Chandra, 1999]. Hence the inclusion of stratospheric ozone changes reduces the tropical RF relative to high latitudes, making these results rather different from those seen in troposphere-only studies, which show the largest ozone RF in the tropics [Gauss *et al.*, 2003].

[32] For aerosols, while black and organic carbon partially offset each other, reduced BC leads to negative forcing over much of the NH with especially large values over China. Sulfate shows forcings that follow the projected regional emissions trends, with a large negative forcing over South Asia where emissions are projected to increase and substantial positive forcings over Europe and especially the US where decreased emissions are projected.

Nitrate, whose emissions change little in the scenario used here, contributes minimally to radiative forcing. Note that the aerosol indirect effects are not included in this discussion as these are integral to the simulated climate and hence their RF cannot be isolated without performing new ensemble simulations.

3.2. Influence of Processes and Present-Day Emissions

[33] Radiative forcing results from other GISS ModelE simulations using either different physical processes and/or emissions are available, and we compare with these to gain insight into the role of emissions uncertainties and the influence of individual physical processes. One set of previous 2030 A1B simulations included ozone photochemistry and sulfate aerosols, but no other aerosols [Unger *et al.*, 2006]. Those simulations did not include stratospheric chemistry, nor did they allow sulfate to be absorbed onto dust surfaces. They were run both with and without climate change (we first examine those without climate change). Another set of A1B 2030 and 2050 simulations looked at sulfate and carbonaceous aerosols [Koch *et al.*, 2007a]. Those simulations did not use coupled oxidants nor did they include climate change, and like those of [Unger *et al.*, 2006] did not include heterogeneous sulfur-dust chemistry (internal mixing). Both other sets of experiments used the same 2030/2050 A1B emissions as used here, and compared with 1995 simulations using the EDGAR 95 inventory.

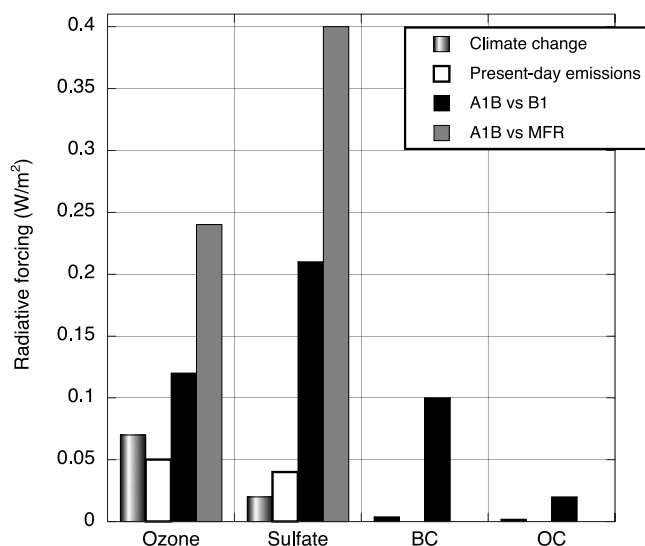


Figure 5. Impact on 2030 radiative forcing (absolute value) of climate change and of using different emission scenarios. Values for climate change are provided as an indication of the uncertainties associated with those processes. Impacts of climate change are taken from this study, using the value at 2050 for ozone, which shows a larger response than at 2030. The present-day emissions shows how the future forcing depends upon the starting emissions by comparing O₃ and SO₄ RF derived using the IIASA 2000 to the EDGAR 1995 emissions.

[34] Comparison with the *Unger et al.* [2006] simulations shows a fairly similar response for ozone, suggesting that the net forcing from including stratospheric changes at 2030 is relatively small (Table 5). This is consistent with the fairly small forcing (-0.06 W/m²) from the larger stratospheric ozone PI to PD changes with this model [*Shindell et al.*, 2006a]. The spatial pattern has changed due to the inclusion of the stratosphere, however, as discussed previously.

[35] The forcings for carbonaceous aerosols are about double those of [*Koch et al.*, 2007b] because of the change in convective scavenging between these model versions described previously. The large difference between the sulfate forcings calculated here and those calculated by [*Unger et al.*, 2006] and [*Koch et al.*, 2007a] reflects absorption of sulfate onto mineral dust surfaces (there may also be a slight residual effect from the erroneously reduced SO₂ oxidation rate that was not fully accounted for by our 1.2 scaling). Inclusion of sulfate uptake onto dust in general improves the agreement between the model and observations [*Bauer and Koch*, 2005]. The magnitude of the sulfate absorption effect is highly uncertain, however, showing strong sensitivity to the uptake mechanism and the dust aerosol size distribution, both of which are difficult to quantify [*Bauer and Koch*, 2005]. Hence it is difficult to know how realistic the forcing reduction due to this process really is. Note that while the two earlier simulations both show larger forcing than that seen here, they differ from one another substantially. This reflects the impact of different oxidant fields in the two simulations (one coupled to the current chemistry, one using offline fields from an older

chemical model) as well as differences in implementing the 2030 emissions. Sulfate's forcing relative to 2000, which was used to drive the transient runs performed here, is closer to the results from the earlier simulations than the forcing relative to 1995. Moreover, since sulfate emissions are projected to return to almost exactly their 1995 value by 2050 (Table 2; albeit with a different spatial distribution), the forcing relative to PD becomes quite small toward the end of the simulations no matter what assumptions about rates and mixing states are used. Hence the sulfate forcing used to drive the transient simulations appears to be plausible for this time period, though quite uncertain.

[36] Examination of the radiative forcings in the runs with and without climate change shows the potential impact of projected warming (Table 5). Comparable simulations, but without stratospheric chemistry by *Unger et al.* [2006] found that projected climate changes reduced the 2030 ozone forcing from .19 to .14 W/m². The reduction in ozone occurred mostly through increased reaction of excited atomic oxygen with the increased tropospheric water vapor found in a warmer climate. Climate change in the current simulations still leads to ozone decreases in the tropics via this mechanism (Figure 2). In the new simulations that include stratospheric chemistry, however, climate change increases ozone's radiative forcing by increasing stratosphere-troposphere exchange and hence ozone near the tropopause (where it most important radiatively) in the extratropics (Figure 2). This is mostly a result of increases in stratospheric ozone, as the *Unger et al.* [2006] simulations included changes in circulation (but not stratospheric ozone) and did not show such large ozone changes near the tropopause. This leads to a maximum impact of climate change on ozone RF of .07 W/m² in 2050 (Table 5).

[37] Climate change reduced sulfate in the *Unger et al.* [2006] simulations, weakening its negative forcing by .02 W/m², as increases in wet and dry removal slightly outweighed increases in oxidation rates, again highlighting the importance of coupled chemistry-aerosol processes. The impact of surface climate change in the current simulations is opposite, slightly increasing sulfate's negative forcing. This is consistent with an increase in extratropical tropospheric ozone in these runs and a decrease in the prior runs without an interactive stratosphere (as ozone aids in sulfur dioxide oxidation both directly and via hydroxyl formation).

[38] Dust emissions decreased slightly ($\sim 5\%$ at 2050, with a 2000 emission of 1580 Tg/yr) in our climate runs, but there was more sulfate on dust (Table 3) suggesting that this played only a minor role in the sulfate forcing response to climate change. The reduction in dust would itself lead to a slight negative forcing (~ 0.02 W/m²). However, emissions in the model respond only to changes in surface wind speeds and soil moisture, and not to changes in sources due to either CO₂ fertilization or climate-induced vegetation changes which have a very uncertain effect on future dust emissions [*Mahowald and Luo*, 2003; *Woodward et al.*, 2005]. The effect of climate change on tropospheric ozone is also fairly uncertain, as chemistry-climate models produce inconsistent results, primarily owing to variations in the response of STE [*Stevenson et al.*, 2006]. Hence it is probably most reasonable to interpret the magnitude of the various climate effects (Figure 5) as indicative of the uncertainty associated with these processes.

Table 6. Methane Lifetime^a

Run	Lifetime, years
2000	9.01
2030	9.96
2050	10.39
2030_clim	9.72
2050_clim	10.01
2050_methane	10.42

^aIncludes calculated photochemical loss (in troposphere and stratosphere) and prescribed 30 Tg/yr loss to soils.

[39] The use of the IIASA 2000 inventory, with reduced emissions compared with the 1995 EDGAR inventory, enhances the projected future forcings for several species. Future ozone increases are larger relative to 2000, and hence the forcing increases by $.05 \text{ W/m}^2$. Future negative forcing from sulfate is similarly enhanced by $.03\text{--}.04 \text{ W/m}^2$ (Figure 5). The different inventories suggest that emissions may have changed rapidly between 1995 and 2000, or the newer inventory may simply be more accurate, though there are still clear biases in some regions [e.g., Pétron *et al.*, 2004; Richter *et al.*, 2005]. In either case, the large differences make future forcing values quite sensitive to the starting year.

[40] A comparable simulation projecting the radiative forcing from nitrate aerosols has also been run, but using the [Streets *et al.*, 2004] 2030 A1B NH_3 emission estimates [Bauer *et al.*, 2007]. Those emissions showed a 29% increase in 2030, much larger than the 5% increase in the IIASA emissions used here. This led to a substantially larger forcing, however the value is still quite small ($-.03 \text{ W/m}^2$, Table 5).

3.3. Influence of Projected Emission Uncertainties

[41] The emissions changes we use are substantially different than common assumptions for some species. The IMAGE model projects slower economic growth than the AIM model, for example. Total energy use is also different in the two models, with 3% greater use in the IMAGE model by 2030, but 9% less usage at 2050. The IMAGE model is less optimistic about emissions controls, leading to greater emissions than in the AIM model for the long-lived gases. For short-lived species, the original SRES A1 IMAGE SO_x emissions were much larger than those of the AIM (or most any other) model (Figure 1). However, the revised IMAGE values used here are quite similar. The IAMs did not project carbonaceous aerosol emissions. The IPCC TAR [Intergovernmental Panel on Climate Change, 2001] suggested scaling future carbonaceous emissions following CO. This leads to large increases with time. At 2050, emissions would increase 38% scaling by CO in the AIM ‘marker’ scenario, with increases spanning 8 to 119% across the A1 IAMs. The newer estimates of [Streets *et al.*, 2004] used here, based on the regional IMAGE model socio-economic output and also including expected technological innovations in emissions controls, instead lead to a substantial decrease in future emissions of carbonaceous aerosols (Figure 1; Table 2). Similarly, NH_3 emissions are sometimes scaled by default to follow N_2O , while the newer IIASA projections have a much slower rate of emissions increase.

[42] Emissions projections of course reflect the underlying socio-economic assumptions used to drive the IAMs. For the SRES, a range of scenarios was developed. While this study looked only at the influence of emissions following an A1B projection, prior GISS modeling [Unger *et al.*, 2006; Koch *et al.*, 2007a] has examined the effects of other scenarios on some of the radiatively active short-lived species. These include the reduced emissions B1 SRES scenario, and one with even more optimistic emissions reductions, the IIASA Maximum Feasible Reduction (MFR) scenario [Dentener *et al.*, 2005]. The impacts of these different scenarios are shown in Figure 5. It is obvious that the A1B scenario used here does not cover all future possibilities. More importantly, it is clear that the forcing is extremely sensitive to the emissions used. In fact, Figure 5 shows that the influence of various physical processes/uncertainties is generally substantially less than the difference between the emission scenarios, at least for the processes and scenarios examined here.

3.4. Methane

[43] The standard 2050 simulations both with and without climate change included methane concentrations prescribed to A1B values from the AIM model, for consistency with the GISS AR4 runs, as noted previously. To investigate the potential uncertainty in the methane value derived by the IAM, we performed an additional 2050 simulation including the full methane cycle in our model. The simulation included prescribed anthropogenic emissions increases from the AIM model and our standard natural emissions [Shindell *et al.*, 2003]. Both the methane emissions from wetlands and the biogenic isoprene emissions were interactive with the climate in this run [Guenther *et al.*, 1995; Shindell *et al.*, 2004]. The distribution of vegetation does not respond to climate change, however, methane’s oxidation rate is calculated by the model’s chemistry scheme. Thus methane can affect its own lifetime, as can other molecules that compete with methane for hydroxyl radicals (the main oxidizing agent), such as isoprene. The simulations included 2050 surface climate (SSTs and sea ice, Table 1). Methane was initialized with estimated 2050 abundances from the AIM model and the simulations were run for 3 years. We note that the IMAGE model projected a continuous increase in methane emissions, rather different from the increase through 2030 and slow decrease thereafter in the AIM model. At 2050, for example, this led to projected anthropogenic methane emissions of 512 Tg/yr in the IMAGE model, substantially greater than the 452 Tg/yr from the AIM model used here (compared with 323 Tg/yr for 2000).

[44] We find that methane emissions from wetlands increase from 195 to 241 Tg/yr while emissions of isoprene increase from 356 to 555 Tg/yr. Additionally, even in the absence of changes in emissions from natural sources, the projected anthropogenic emissions of ozone precursors (including methane itself) increase the lifetime of methane while climate change reduces it via increased temperature and water vapor (Table 6). The effect of precursor emissions is stronger in our scenario, so that the net effect of anthropogenic emissions and climate changes is to increase methane’s lifetime. When natural emissions are also allowed to respond to climate change, increased competition from isoprene and increased methane emissions from wet-

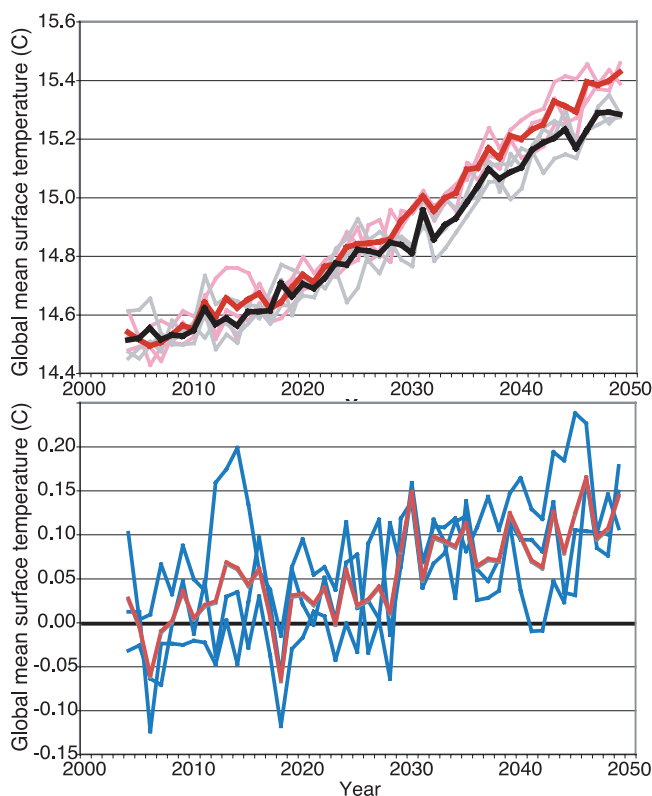


Figure 6. Global mean annual average surface air temperature ($^{\circ}\text{C}$) in the transient climate simulations. Time series for both the runs with short- and long-lived species (red) and long-lived species only (black) are shown (top panel, thick line is the ensemble mean). Their difference shows the impact of short-lived species only (bottom panel). Differences are presented for the individual runs versus individual controls (blue) and for the ensemble average versus ensemble control (red).

lands lead to further increases in methane's lifetime (Table 6) and enhanced methane abundance.

[45] The 2050_methane simulation had a global mean surface methane value of 2.86 ppmv in year 3, with sources exceeding sinks by 80 Tg/yr (a growth rate that may reflect an overestimate of the loss rate in the AIM model used in the initial guess). Extrapolating the change in methane out to equilibrium using an exponential fit to the three years of model results yields a 2050 value of 3.21 ppmv.

[46] We calculate radiative forcings using the TAR calculation (Table 6.2 in [Ramaswamy *et al.*, 2001]) assuming an increase in N_2O from 316 to 350 ppb in 2050 following the A1B AIM 'marker' scenario. The 2050 forcing from the AIM A1B methane would be 0.22 W/m^2 while using the larger methane concentrations of 2.86 or 3.21 ppmv calculated with our model gives 0.36 or 0.46 W/m^2 , respectively. Of course it is difficult to estimate methane's abundance at a particular time without performing a full transient methane simulation. However, uncertainty in the forcing from methane appears to be at least one to two tenths of a watt per meter squared. Note that use of the $\sim 40\%$ larger anthropogenic methane emission increase from the IMAGE model would have led to a substantially larger forcing. Should the

results of our modeling of the methane cycle prove to be fairly robust, this would imply that future positive forcing from methane may be substantially larger than current estimates based on IAM projections. As noted previously, there is also a substantial uncertainty in the projections of anthropogenic methane emissions given the stabilization of the growth rate in recent years.

4. Climate Response

4.1. Global Mean Annual Average

[47] Despite the weak direct climate forcing from short-lived species (Table 5), global mean annual average surface air temperature increases approximately $.07^{\circ}\text{C}$ by 2030 and around $.13^{\circ}\text{C}$ near 2050 due to short-lived species (Figure 6). The warming substantially exceeds the standard deviation, which is about 0.04°C for the decadal average ensemble mean temperature. We attribute the enhanced warming relative to the direct forcing times the climate sensitivity ($.02 \text{ W/m}^2 \times 0.6^{\circ}\text{C}/(\text{W/m}^2) = 0.01^{\circ}\text{C}$ at 2050) largely to the reduction of the aerosol indirect effect. As noted previously, since the aerosol-cloud interactions are integral to the simulated climate, it is not possible to fully diagnose their RF without performing new ensemble simulations. We can, however, get a very rough idea of the RF magnitude by examining the change in aerosols relative to the PI to PD changes. We calculate the change in number concentration of soluble aerosols at 2030 and 2050 relative to 2000, as the aerosol indirect effect parameterization is based on this quantity (see Section 2.3). The ratio of change in projected number concentration of soluble aerosols to the PI to PD change allows us to estimate RF relative to the -1 W/m^2 PI to PD value. This yields aerosol indirect effect RF estimates of $\sim .13 \text{ W/m}^2$ at 2030 and $\sim .21 \text{ W/m}^2$ at 2050 (both relative to 2000). Our calculation is only approximate, however, as we use global mean concentrations, while the change in cloud cover will depend upon local number concentrations.

[48] Given the model's climate sensitivity to CO_2 of 0.6°C per W/m^2 , and that the fixed-SST efficacy of the short-lived species is within 20% of the CO_2 efficacy [Hansen *et al.*, 2005], we would expect this indirect forcing combined with the direct forcing of $.02 \text{ W/m}^2$ at 2050 to lead to a warming of $\sim .14^{\circ}\text{C}$, roughly consistent with what actually happened (though we would not expect the climate to have fully responded to the forcing yet, so the equilibrium climate sensitivity is an overestimate). Thus it is certainly plausible that warming caused by a reduction in the aerosol indirect effect contributes substantially to the temperature increases seen in these simulations. Note also that for spatially inhomogeneous RFs, the global mean value does not always provide a good indication of the response. For example, a zero global mean RF can give a non-zero global mean surface temperature response [Berntsen *et al.*, 2005].

[49] Further evidence for the role of the indirect effect comes from the temporal behavior of the surface temperature. Modeled global mean warming was more rapid during the 2030 to 2050 period ($.03^{\circ}\text{C}/\text{decade}$) than during 2000 to 2030 ($.02^{\circ}\text{C}/\text{decade}$, Figure 6), despite a miniscule increase in the direct forcing (Table 5). This is consistent with the trend in the number concentration of soluble aerosols during

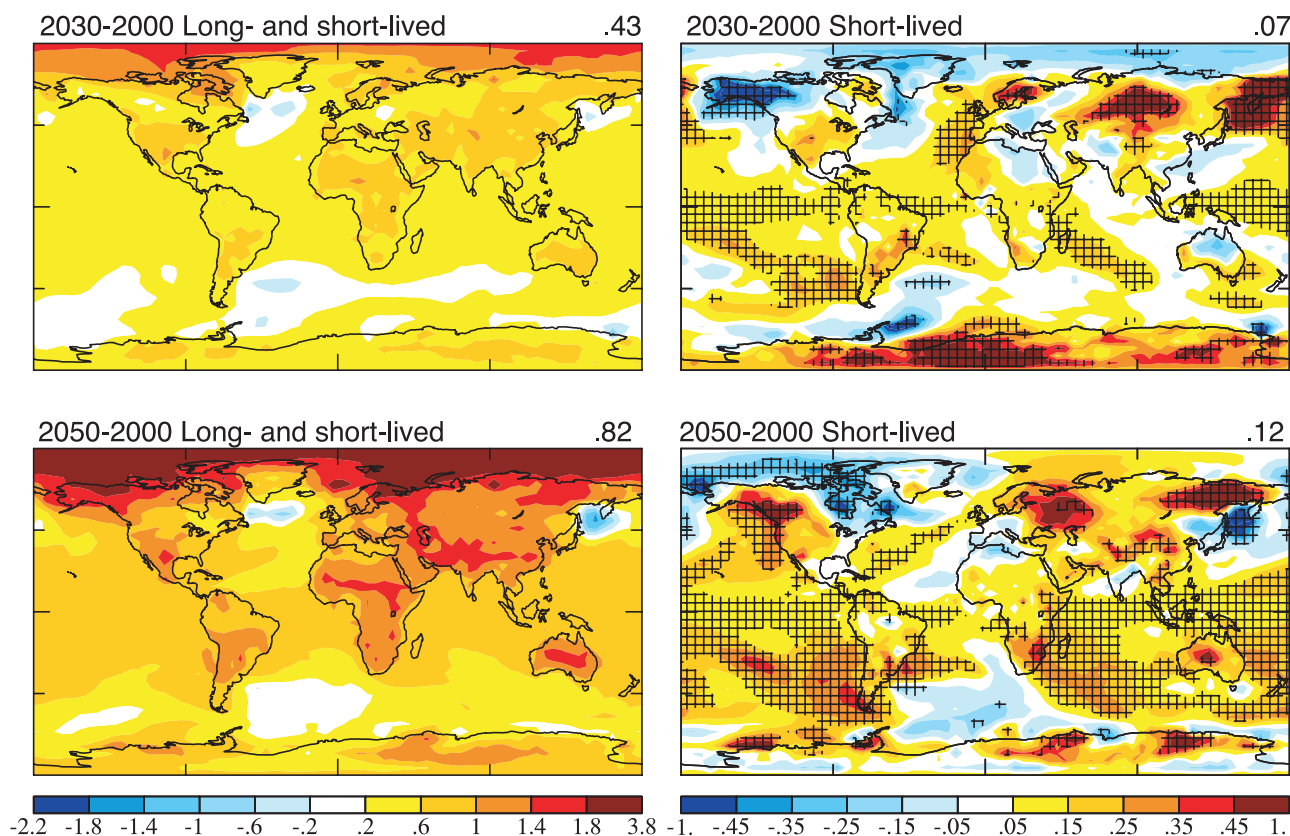


Figure 7. Ensemble mean changes in annual average surface air temperature ($^{\circ}\text{C}$) in the transient climate simulations with projected long- and short-lived species (left column) and the difference between the runs with long- and short-lived species minus long-lived only (right column). Differences between multiyear averages are shown using 2003–2008 for 2000, 2028–2033 for 2030, and 2040–2050 for 2050. Values in the upper right corners give the global mean. Hatching indicates 95% significance in the right column. All colored values in the left column are significant.

these simulations. We find that from 2000 to 2030, reduction of OC plays the largest role, but that $\sim 50\%$ of this is offset by the increased sulfate during this time. From 2030 to 2050, global sulfate, OC, and BC all decrease, with the small increase in nitrate offsetting only a minor portion of this. Overall, the reduction in the number concentration of soluble aerosols is $\sim 50\%$ larger in 2050 than in 2030 (6% in 2030 and 11% in 2050). Given that the logarithmic dependence of cloud droplet number concentration on soluble aerosol concentration means that aerosol changes are more effective at lower densities, an even larger change in the forcing during the latter part of the simulations relative to the earlier part must have taken place. This faster reduction of the aerosol indirect effect is qualitatively consistent with the approximate 50% enhancement of the rate of warming during the latter 20 years of the simulation. As noted previously, analysis of the global budgets provide only a very rough picture of the actual aerosol indirect effect. Additionally, some of the reduction in the warming rate during the early part of the run results from the lag in climate response to RF.

[50] Comparison between the effects of the long-lived greenhouse gases and the short-lived species shows that the long-lived clearly dominate (Figure 7). We reiterate that

methane is included among the long-lived species in assessing climate response. Nevertheless, the projected changes in short-lived species play a substantial role in the overall trend, augmenting the annual average warming by 19% around 2030 and by 17% near 2050. This percentage may be slightly on the high side as WMGHG emissions increase by $\sim 20\%$ more in the IMAGE model than in the AIM model used here for WMGHGs. A response to WMGHGs that was 20% larger would reduce the enhancement due to short-lived species by only a few percent, however (from $\sim 18\%$ to 15%). The warming from short-lived species is attributable to positive forcings from ozone and the aerosol indirect effect, with a lesser contribution from OC, which are partially offset by negative forcings from BC and sulfate (Table 5). It is worth noting that all these forcings are of the same order of magnitude, differing by only a factor of 3 or 4, and hence any of these can substantially influence the net RF.

4.2. Regional and Seasonal Responses

[51] The spatial pattern of the climate response to short-lived species bears relatively little resemblance to the direct radiative forcing (Figure 7 versus Figure 3). While the forcing is largest at high latitudes and over some tropical land areas, the response is clearest over tropical and

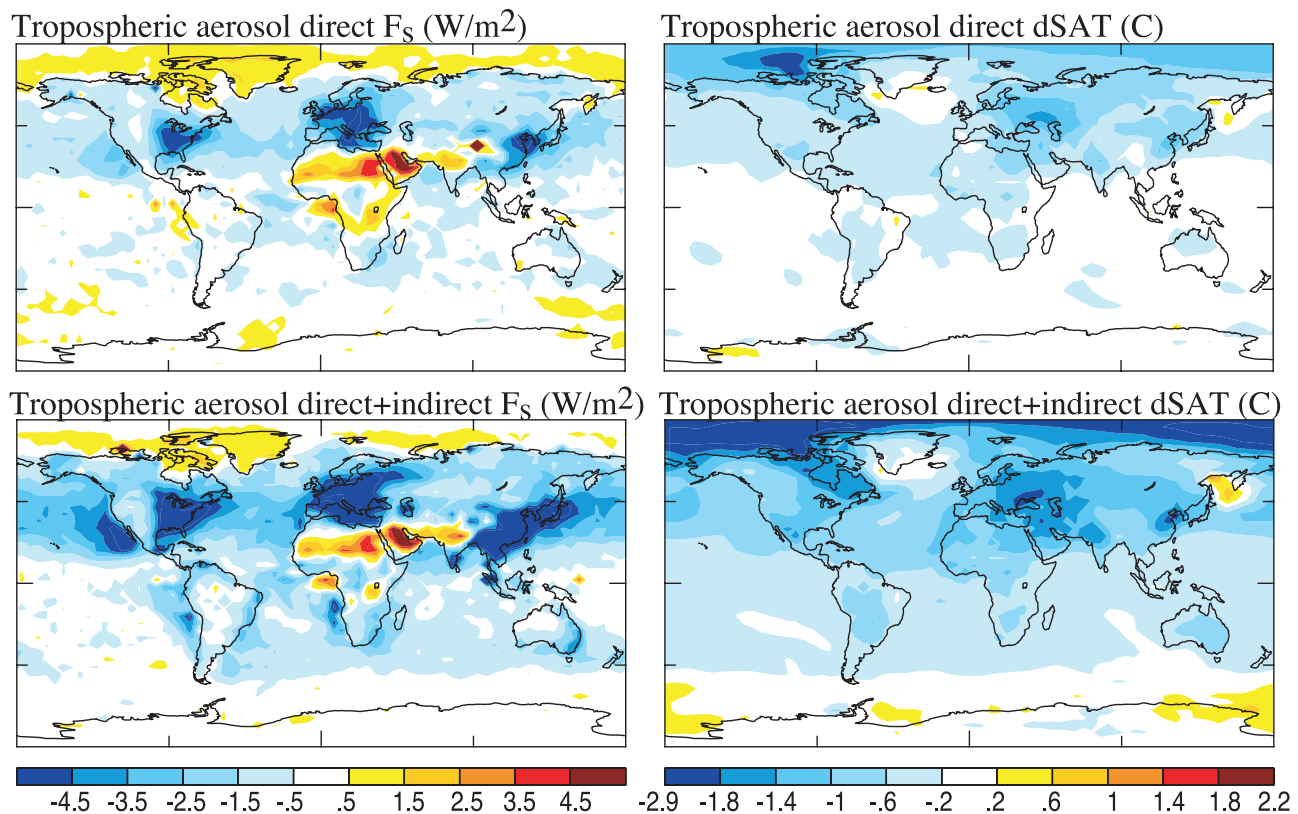


Figure 8. Ensemble mean annual average 1880–2003 radiative forcing (F_s , the top-of-the-atmosphere forcing with fixed SSTs and sea-ice, left column) and the surface air temperature (SAT) response ($^{\circ}\text{C}$, local linear trends, right column) from 5-member ensemble simulations driven by tropospheric aerosols including their direct radiative effect only (top row) and both their direct and indirect (via cloud cover) effects (bottom row). Similar results were presented in [Hansen *et al.*, 2005] for single-member simulations.

subtropical oceans (statistical significance for surface temperature is calculated by comparing the mean change between future and present with the variability during the present, e.g., using the 18 years of 2003–2008 in the 3 ensemble members for Figure 7). Though the aerosol indirect effect plays a role in these differences, it cannot account for all of the spatial mismatch between forcing and response. For example, over South Asia and Africa north of the equator, the aerosol indirect forcing should enhance the direct forcing as both are primarily due to increased sulfate (Figure 4). Hence both direct and indirect forcing should induce cooling, yet this does not happen. Similarly, there are reductions in both BC and sulfate over the eastern US, which will lead to a reduced aerosol indirect effect there. As the net direct forcing there is positive (Figure 3), both should cause warming, but this also does not take place.

[52] Both the conclusion that the response does not follow the forcing and that the aerosol indirect effect cannot explain this are supported by analysis of historical GISS climate simulations [Hansen *et al.*, 2007b]. Transient ensemble climate simulations for 1880–2003 including the direct effects of tropospheric aerosols and a separate ensemble including both aerosol direct and indirect effects both show surface temperature response patterns distinctly different from the imposed forcings (Figure 8). Some regions, such as North Africa, Arabia and the Arctic, show

responses of the opposite sign to the forcing. Midlatitude regions including East Asia and the eastern US show temperature responses similar to the zonal mean despite very large forcings localized in those areas. Thus it is clear that even when the aerosol indirect forcing is including, the local response does not closely follow the forcing over much of the globe. These results are consistent with earlier modeling studies examining the response to different forcings than those investigated here [Boer and Yu, 2003; Berntsen *et al.*, 2005; Hansen *et al.*, 2005].

[53] On a hemispheric scale, the response does seem to be related to the projected future forcing from short-lived

Table 7. Hemispheric RF (W/m^2) and Surface Air Temperature Response ($^{\circ}\text{C}$)^a

	NH RF	NH SAT	SH RF	SH SAT
2030 Short-lived	−.17 (~.21)	.07	.17 (~.05)	.08
2030 Long-lived	1.38	.45	1.38	.27
2050 Short-lived	−.14 (~.34)	.09	.18 (~.08)	.14
2050 Long-lived	2.40	.86	2.40	.54

^aRF is direct forcing from short- or long-lived species, with values in parentheses giving a very rough estimate of the RF from the aerosol indirect effect using the calculation described in the text and assuming that 80% of the global effect is in the NH. RF due to long-lived species is based on the AIM A1B results.

species, though the relationship depends on the poorly quantified aerosol indirect effect. Because of stronger positive ozone forcing in the SH and stronger negative aerosol forcing in the NH, the net direct forcing is $\sim 0.3 \text{ W/m}^2$ greater in the SH than the NH for 2030–2050 (Table 7 and 5). Some of this difference is removed by the stronger reduction in the aerosol indirect effect in the NH, however the SH RF is always greater than in the NH. Consistent with this enhanced RF, the SH warms by $.01\text{--}.05^\circ\text{C}$ more than the NH. Thus at 2050, the hemispheric mean warming from short-lived species is $\sim 55\%$ greater in the SH than in the NH. In contrast, the WMGHGs induce roughly 60% more warming in the NH than in the SH, largely as a result of stronger positive feedbacks since the RFs in the two hemispheres are roughly equal. Hence the greater SH response to short-lived species is clearly a result of the inhomogeneous forcings rather than inhomogeneous feedbacks.

[54] The seasonal responses to the projected changes in short-lived species show some significant (at 95%, taking into account the local autocorrelation of $\sim 1\text{--}2$ year) and stable features, including warming over large areas of the oceans other than the Arctic, cooling of the Arctic during boreal spring (significant only in some portions) and warming of the Antarctic during austral summer (Figure 9). The NH mid to high latitude response during the boreal winter bears the signature of an enhanced westerly circulation (a positive shift in the Northern Annular Mode or Arctic Oscillation), which increases by $\sim 0.4 \text{ m/s}$ near the surface around $50\text{--}55^\circ\text{N}$ during this season comparing 2045–2050 with 2003–2008 (not shown) and is statistically significant at the 95% level. This is similar to the response to a warmer climate seen in several other model studies [Miller *et al.*, 2006b]. In contrast, WMGHGs induce an amplified (relative to the global mean) boreal winter warming through most of the Northern high latitudes (Figure 10), including North America, Eurasia and the Arctic Ocean (enhanced westerly flow is also induced by WMGHGs, but it is not such a dominant factor as in the short-lived species response). The response to WMGHGs also includes strong warming over eastern Africa and much of central Asia that is not seen in the response to short-lived species. Thus the regional response to the short-lived species is clearly distinct from the response to WMGHGs.

[55] We can compare the seasonal responses to short-lived species with their forcing, focusing on the boreal winter when some of the most significant regional responses were seen. Sulfate provides some positive forcing over North America, especially in the eastern US, but the direct high latitude forcing from short-lived species is dominated by the forcing from ozone (Figure 10). This positive ozone forcing is mostly due to stratospheric ozone, as the forcing remains comparably large even in summer (not shown) when tropospheric ozone formed from midlatitude pollution is largely destroyed chemically before reaching the Arctic. As with the annual average, the climate response generally does not closely resemble the direct forcing (though again, the aerosol indirect effect contributes to this mismatch).

[56] Sizable areas in the Arctic cool by more than 0.5°C during NH winter and spring in 2030 (visible in the annual average as well (Figure 7)), and during NH spring in 2050 (Figure 9), all of which are statistically significant in at least some areas. This may be related to a reduction in high-

latitude aerosol indirect effect longwave forcing. It is possible, however, that cooling from short-lived species results from their overall negative forcing in the NH extratropics which is then communicated dynamically to the Arctic [Shindell, 2007].

[57] In contrast, the Antarctic is far removed from most anthropogenic pollution, and thus there is little aerosol forcing there (Figure 4). As a result, there is no aerosol-induced cooling and instead climate there shows substantial warming from short-lived species, maximizing in austral summer (Figure 9). This warming results from stratospheric ozone recovery due to both its direct radiative impact (Figure 4) and via a decrease in the westerly winds that isolate the Antarctic from warmer air at lower latitudes which is driven by ozone recovery [Kindem and Christiansen, 2001; Gillett and Thompson, 2003; Shindell and Schmidt, 2004]. In this region, the WMGHGs also induce an enhanced warming relative to the global mean, but the relative enhancement is less than for the short-lived species as they have a positive radiative forcing (warming) but increase the strength of the westerlies (cooling) [Fyfe *et al.*, 1999; Kushner *et al.*, 2001; Shindell and Schmidt, 2004; Miller *et al.*, 2006b].

[58] Examination of the precipitation response to short-lived species shows changes primarily over the tropical oceans (not shown), with little correlation to either forcing or to aerosol distributions. Precipitation increases over East Asia, where aerosol changes are large, but the increase is not statistically significant. Note that since the parameterized indirect effect does not include aerosol effects on precipitation through changes in autoconversion (conversion of cloud water to rain), aerosols can only affect precipitation via their direct impact on local heating. This is quite sensitive to vertical distributions of aerosols (especially the absorbing fraction), hence the potential aerosol modification of precipitation needs to be explored in greater detail with accompanying sensitivity studies that are beyond the scope of this paper.

5. Conclusions

[59] While numerous prior studies have examined the potential changes in the future abundance of short-lived radiatively active species, they have primarily produced estimates of concentration [Prather *et al.*, 1999] or radiative forcing [Charlson *et al.*, 1992; Gauss *et al.*, 2003; Stevenson *et al.*, 2006; Unger *et al.*, 2006; Koch *et al.*, 2007a] rather than climate response. Although the radiative forcing may be adequate for estimating the global mean climate response, the simulations carried out here suggest that substantial hemispheric and regional climate responses can take place that are distinctly different from the responses to long-lived species. Indeed, the global mean response to inhomogeneous forcings can be non-zero even if the RF is zero [Berntsen *et al.*, 2005] due to differing regional climate sensitivities. Such effects were seen in our study in the NH/SH asymmetry of warming, and over Asia, the Arctic and the Antarctic.

[60] The simulations also showed, however, that in most cases regional climate responses bear little resemblance to the spatial pattern of the direct forcing. Thus despite projected negative direct forcing of $2\text{--}4 \text{ W/m}^2$ over much of East and South Asia, where the aerosol indirect effect

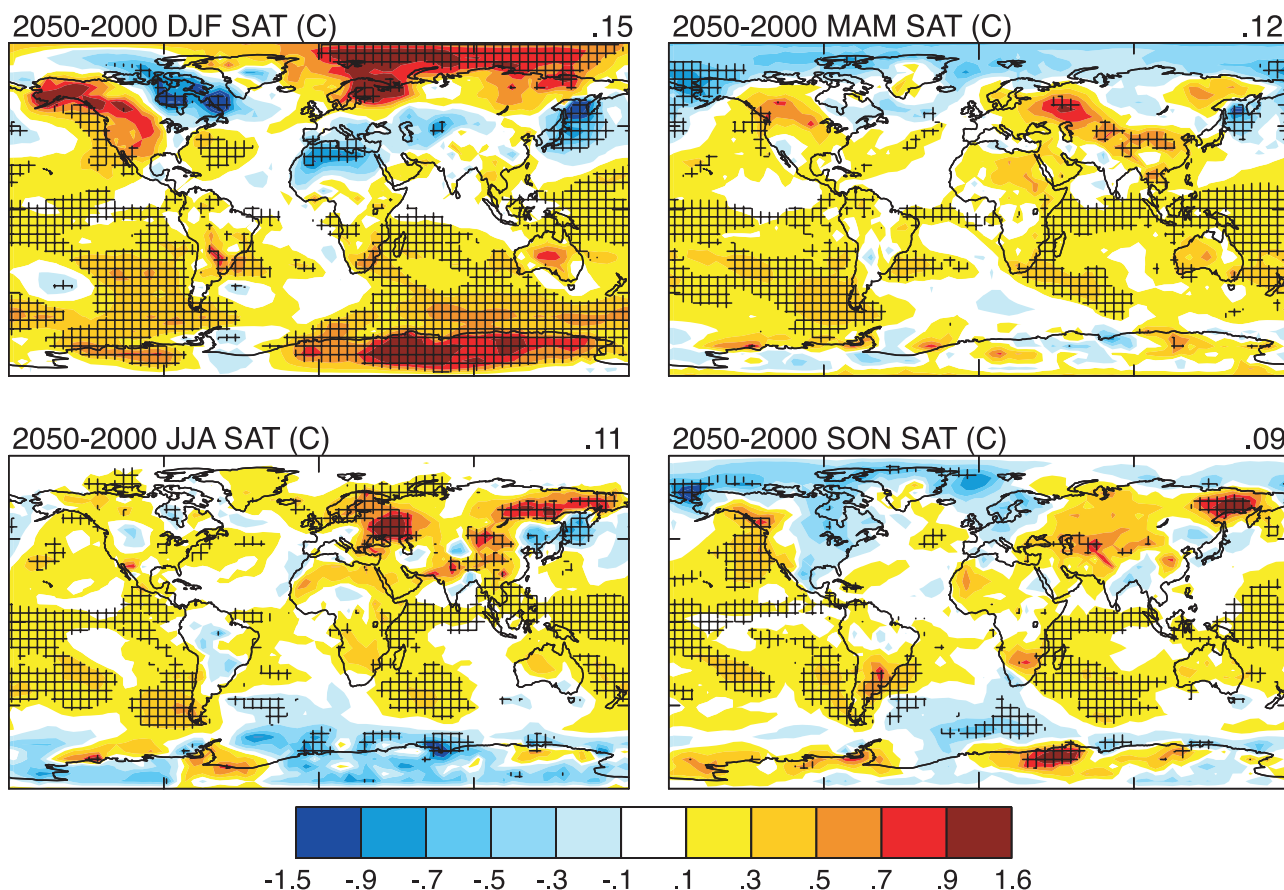


Figure 9. Ensemble mean seasonal average surface air temperature (°C) changes induced by the short-lived species near 2050 based on the last 11 years of the transient ensemble simulations. Numbers in the upper right corners give the global mean. Hatching indicates 95% significance.

also causes a negative forcing, surface temperatures there showed a slight warming consistent with the global average response. This suggests that regional climates are typically dominated by the effects of atmospheric circulation and the nearby ocean surface temperatures rather than by local radiative forcing. We note that there is evidence that short-lived species can modify circulation in the ocean [Delworth and Dixon, 2006] and atmosphere [Kim et al., 2006], so that the regional forcing may have important regional consequences. Our conclusion is simply that the regional forcing may be of limited use in predicting the regional climate response.

[61] Current climate models are able to reproduce global mean temperature trends over the past 100 years quite well, but have considerably more difficulty in reproducing the regional patterns of 20th century climate change [Intergovernmental Panel on Climate Change, 2001]. Potential reasons for this difficulty are (1) that models lack appropriate representations of some physical processes important in the dynamic response to climate forcings, (2) that inhomogeneous forcings from aerosols are poorly represented, or (3) that the observed regional climate changes are largely unforced. Our results show a lack of specific regional climate response to even large aerosol forcing comparable in size to that seen over the past 30 years in most parts of the world. This suggests that the second explanation is less likely than might have previously been supposed.

[62] Several processes were explored here but not included in our transient climate simulations. Those showing the most significant potential effects were the impact of climate change on ozone, and the influence of emissions and changes in the oxidizing capacity of the troposphere on methane. These two processes increased the forcing by $.07 \text{ W/m}^2$ and $\sim 2 \text{ W/m}^2$, respectively, in 2050 in our tests. As the methane response comes about at least in part from the influence of the short-lived species on its oxidation, we believe it is useful to consider methane along with these others. Note that the climate change induced by the short-lived species is not included in the SSTs used to drive the methane simulation and would further alter both natural emissions and oxidation rates, so that our calculated methane RF is only a rough approximation. Taking into account the climate sensitivity of our model, these potential enhancements to the ozone and methane forcings imply an additional $.16^\circ\text{C}$ global mean annual average equilibrium warming ($\sim 0.1^\circ\text{C}$ assuming the response was not fully realized). This would make the total warming from short-lived species plus the warming from enhanced methane relative to the standard A1B scenario about $0.20\text{--}0.25^\circ\text{C}$ at 2050. This is $\sim 33\%$ of the response to WMGHGs at that time. These results further underline the potential importance of the short-lived species for climate projection.

[63] We also emphasize that some of the processes included in our simulations have large uncertainties. Among

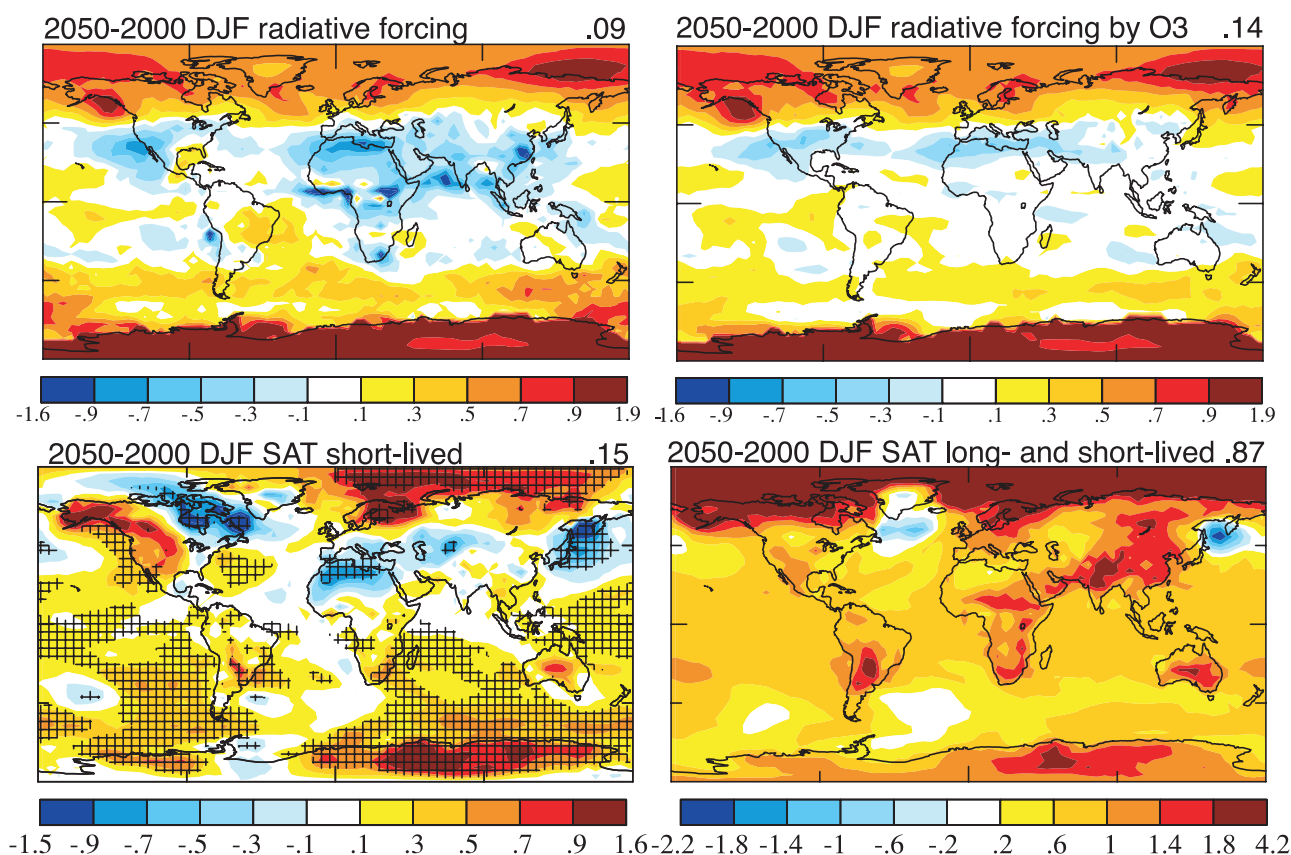


Figure 10. Northern winter (Dec-Feb) instantaneous tropopause radiative forcing (W/m^2) from all short-lived species (upper left) and from ozone alone (upper right), surface air temperature (SAT) response ($^{\circ}\text{C}$) to all short-lived species (lower left), and the SAT response to short- and long-lived species changes (lower right). Values in the upper right give the global mean. All colored positive values are significant in the DJF SAT response shown in the lower right, while hatching indicates 95% significance in the lower left.

the most important to the current results may be the influence of sulfate absorption onto dust, which decreases the sulfate forcing by $\sim 40\%$ between 2000 and 2030 in comparable simulations by [Bauer *et al.*, 2007]. However, the absorption rates are quite uncertain, hence this process could in reality be substantially smaller. Mixing of additional aerosol types is also highly uncertain, but is known to occur in the atmosphere and would also affect the magnitude of aerosol forcings. Additionally, many aspects of aerosol-cloud interactions are poorly known, and our highly parameterized approach is quite crude. Thus a substantial portion of the response in our simulations results from processes with a relatively low level of scientific understanding. Hence the effects of these physical processes provide an indication of the uncertainties associated with projections of short-lived species. While the results suggest a substantial impact of short-lived species on climate, there is less evidence of a strong impact of climate change on the short-lived species other than ozone (and methane). Hence while it would be preferable to calculate the composition and climate changes interactively, using offline composition fields to drive the climate simulations seems likely to capture the primary aspects of the response (though further work is required to fully evaluate this).

[64] It is also clear that some potential processes have not been included yet. An example is the future dust loading, which can influence the composition of other short-lived species and can also be influenced by those species (e.g., via changes in solubility due to nitrate or sulfate uptake [Bauer and Koch, 2005]). Dust emission will respond to vegetation changes as the climate warms. Arid regions contract as a result of fertilization of plants by increased CO_2 , reducing emission according to [Mahowald and Luo, 2003], while source regions expand as a result of global warming and reduced rainfall, and thus increase emission in another study [Woodward *et al.*, 2005]. Note that the actual trend will depend upon local changes in climate, and especially rainfall, which is among the least robust aspect of current climate projections. No dust changes were included in the current transient climate simulations.

[65] Further work is clearly required to better characterize the physical processes governing the abundance and radiative properties of short-lived species. Our study highlights the importance of uncertainties such as mixing of aerosol types or the effect of climate change on stratosphere-troposphere exchange. However, for all the species and processes examined here, the impact of variations between future emissions scenarios always exceeded that of physical

uncertainties. Thus projections of the climate impact of short-lived species appear to be dominated by uncertainty in socio-economic development rather than the sizable uncertainties in physical processes (though multiple physical uncertainties could together conceivably outweigh the influence of the scenarios). Nonetheless, to explore the climate response to a particular socio-economic projection, our results clearly demonstrate that short-lived species should be taken into account. For the A1B scenario examined here, they increased the warming from long-lived species by $\sim 15\text{--}20\%$. This suggests that much greater attention should be paid to including realistic evolution of short-lived species in a potential IPCC AR5 than was done in the AR4.

References

- Andreae, M. O., and P. Merlet (2001), Emission of trace gases and aerosols from biomass burning, *Global Biogeochem. Cycles*, **15**, 955–966.
- Bauer, S. E., and D. Koch (2005), Impact of heterogeneous sulfate formation at mineral dust surfaces on aerosol loads and radiative forcing in the Goddard Institute for Space Studies general circulation model, *J. Geophys. Res.*, **110**, D17202, doi:10.1029/2005JD005870.
- Bauer, S. E., M. I. Mishchenko, A. Lacis, S. Zhang, J. Perlwitz, and S. M. Metzger (2006), Do sulfate and nitrate coatings on mineral dust have important effects on radiative properties and climate modeling?, *J. Geophys. Res.*, **112**, D06307, doi:10.1029/2005JD006977.
- Bauer, S. E., D. Koch, N. Unger, S. M. Metzger, D. T. Shindell, and D. Streets (2007), Nitrate aerosols today and in 2030: Importance relative to other aerosol species and tropospheric ozone, *Atmos. Chem. Phys. Discuss.*, **5**, 5553–5593.
- Berntsen, T. K., J. S. Fuglestad, M. M. Joshi, K. P. Shine, N. Stuber, M. Ponater, R. Sausen, D. A. Hauglustaine, and L. Li (2005), Response of climate to regional emissions of ozone precursors: Sensitivities and warming potentials, *Tellus B*, **57**, 283–304.
- Boer, G., and B. Yu (2003), Climate sensitivity and response, *Clim. Dyn.*, **20**, 415–429.
- Bousquet, P., et al. (2006), Contribution of anthropogenic and natural sources to atmospheric methane variability, *Nature*, **443**, 439–442.
- Charlson, R. J., S. E. Schwartz, J. M. Hales, R. D. Cess, J. A. J. Coakley, J. E. Hansen, and D. J. Hofmann (1992), Climate forcing by anthropogenic aerosols, *Science*, **255**, 423–430.
- Collins, W. J., R. G. Derwent, B. Garnier, C. E. Johnson, M. G. Sanderson, and D. S. Stevenson (2003), Effect of stratosphere-troposphere exchange on the future tropospheric ozone trend, *J. Geophys. Res.*, **108**(D12), 8528, doi:10.1029/2002JD002617.
- Delworth, T. L., and K. W. Dixon (2006), Have anthropogenic aerosols delayed a greenhouse gas-induced weakening of the North Atlantic thermohaline circulation?, *Geophys. Res. Lett.*, **33**, L02606, doi:10.1029/2005GL024980.
- Dentener, F. D., D. S. Stevenson, J. Cofala, R. Mechler, M. Amann, P. Bergamaschi, F. Raes, and R. G. Derwent (2005), Tropospheric methane and ozone in the period 1990–2030: CTM calculations on the role of air pollutant and methane emissions controls, *Atmos. Chem. Phys.*, **5**, 1731–1755.
- Dentener, F., et al. (2006), The global atmospheric environment for the next generation, *Environ. Sci. Technol.*, **40**, 3586–3594.
- Dlugokencky, E. J., S. Houweling, L. Bruhwiler, K. A. Masarie, P. M. Lang, J. B. Miller, and P. P. Tans (2003), Atmospheric methane levels off: Temporary pause or a new steady-state?, *Geophys. Res. Lett.*, **30**(19), 1992, doi:10.1029/2003GL018126.
- Fiore, A. M., D. Jacob, B. Field, D. G. Streets, S. D. Fernandes, and C. Jang (2002), Linking ozone pollution and climate change: The case for controlling methane, *Geophys. Res. Lett.*, **29**(19), 1919, doi:10.1029/2002GL015601.
- Fyfe, J. C., G. J. Boer, and G. M. Flato (1999), The Arctic and Antarctic Oscillations and their protected changes under global warming, *Geophys. Res. Lett.*, **26**, 1601–1604.
- Gauss, M., et al. (2003), Radiative forcing in the 21st century due to ozone changes in the troposphere and the lower stratosphere, *J. Geophys. Res.*, **108**(19), 4292, doi:10.1029/2002JD002624.
- Gettelman, A., J. R. Holton, and K. H. Rosenlof (1997), Mass fluxes of O₃, CH₄, N₂O, and CF₂Cl₂ in the lower stratosphere calculated from observational data, *J. Geophys. Res.*, **102**, 19,149–19,159.
- Gillet, N. P., and D. W. J. Thompson (2003), Simulation of recent Southern Hemisphere climate change, *Science*, **302**, 273–275.
- Guenther, A., et al. (1995), A global model of natural volatile organic compound emissions, *J. Geophys. Res.*, **100**, 8873–8892.
- Hansen, J., et al. (2005), Efficacy of Climate Forcings, *J. Geophys. Res.*, **110**, D18104, doi:10.1029/2005JD005776.
- Hansen, J., et al. (2007a), Dangerous human-made interference with climate: A GISS modelE study, *Atmos. Chem. Phys.*, **7**, 2287–2312.
- Hansen, J., et al. (2007b), Climate simulations for 1880–2003 with GISS modelE, *Clim. Dyn.*, in press, doi:10.1007/s00382-00007-00255-00388.
- IMAGE Team (2001), *The Image 2.2 implementation of the SRES scenarios*, National Institute for Public Health and the Environment, Bilthoven, The Netherlands.
- Intergovernmental Panel on Climate Change (2001), *Climate Change 2001*, 881 pp., Cambridge Univ. Press, Cambridge.
- Kim, M.-K., W. K. M. Lau, M. Chin, K.-M. Kim, Y. C. Sud, and G. K. Walker (2006), Atmospheric teleconnection over Eurasia induced by aerosol radiative forcing during boreal spring, *J. Clim.*, **19**, 4700–4718.
- Kindem, I. T., and B. Christiansen (2001), Tropospheric response to stratospheric ozone loss, *Geophys. Res. Lett.*, **28**, 1547–1551.
- Kinne, S., et al. (2006), An AeroCom initial assessment - Optical properties in aerosol component modules of global models, *Atmos. Chem. Phys.*, **6**, 1815–1834.
- Koch, D., G. A. Schmidt, and C. Field (2006), Sulfur, sea salt and radionuclide aerosols in GISS ModelE, *J. Geophys. Res.*, **111**, D06206, doi:10.1029/2004JD005550.
- Koch, D., T. Bond, D. Streets, N. Bell, and G. R. van der Werf (2007a), Global impacts of aerosols from particular source regions and sectors, *J. Geophys. Res.*, **112**, D02205, doi:10.1029/2005JD007024.
- Koch, D., T. Bond, D. Streets, and N. Unger (2007b), Linking future aerosol radiative forcing to shifts in source activities, *Geophys. Res. Lett.*, **34**, L05821, doi:10.1029/2006GL028360.
- Kushner, P. J., I. M. Held, and T. L. Delworth (2001), Southern Hemisphere atmospheric circulation response to global warming, *J. Clim.*, **14**, 2238–2249.
- Mahowald, N. M., and C. Luo (2003), A less dusty future?, *Geophys. Res. Lett.*, **30**(17), 1903, doi:10.1029/2003GL017880.
- Menon, S. A., D. Del Genio, D. Koch, and G. Tselioudis (2002), GCM simulations of the aerosol indirect effect: Sensitivity to cloud parameterization and aerosol burden, *J. Atmos. Sci.*, **59**, 692–713.
- Metzger, S., N. Mihalopoulos, and J. Lelieveld (2006), Importance of mineral cations and organics in gas-aerosol partitioning of reactive nitrogen compounds: case study based on {MINOS} results, *Atmos. Chem. Phys.*, **6**, 2549–2567.
- Miller, R. L., et al. (2006a), Mineral Dust Aerosols in the NASA Goddard Institute for Space Studies ModelE AGCM, *J. Geophys. Res.*, **111**, D06208, doi:10.1029/2005JD005796.
- Miller, R. L., G. A. Schmidt, and D. T. Shindell (2006b), Forced variations of annular modes in the 20th century Intergovernmental Panel on Climate Change Fourth Assessment Report models, *J. Geophys. Res.*, **111**, D18101, doi:10.1029/2005JD006323.
- Nakicenovic, N., et al. (2000), *IPCC Special Report on Emissions Scenarios*, 570 pp., Cambridge Univ. Press, Cambridge, UK.
- Oltmans, S. J., et al. (1998), Trends of ozone in the troposphere, *Geophys. Res. Lett.*, **25**, 139–142.
- Penner, J. E., J. Quaas, T. Storelvmo, T. Takemura, O. Boucher, H. Guo, A. Kirkevåg, J. E. Kristjánsson, and Ø. Seland (2006), Model intercomparison of indirect aerosol effects, *Atmos. Chem. Phys. Discuss.*, **6**, 1579–1617.
- Pétron, G., C. Granier, B. Khattatov, V. Yudin, J.-F. Lamarque, L. Emmons, J. Gille, and D. P. Edwards (2004), Monthly CO surface sources inventory based on the 2000–2001 MOPITT satellite data, *Geophys. Res. Lett.*, **31**, L21107, doi:10.1029/2004GL020560.
- Prather, M., et al. (1999), Fresh air in the 21st century?, *Geophys. Res. Lett.*, **30**, 1100, doi:10.1029/2002GL016285.
- Ramaswamy, V., et al. (2001), Radiative forcing of climate change, in *Climate Change 2001*, edited by J. T. Houghton, pp. 349–416, Cambridge Univ. Press, Cambridge.
- Rayner, N. A., D. E. Parker, E. B. Horton, C. K. Folland, L. V. Alexander, D. P. Rowell, E. C. Kent, and A. Kaplan (2003), Global analyses of sea surface temperature, sea ice, and night marine air temperature since the late nineteenth century, *J. Geophys. Res.*, **108**(D14), 4407, doi:10.1029/2002JD002670.
- Richter, A., J. P. Burrows, H. Nuss, C. Granier, and U. Niemeier (2005), Increase in tropospheric nitrogen dioxide over China observed from space, *Nature*, **437**, 129–132.
- Russell, G. L., J. R. Miller, and D. Rind (1995), A coupled atmosphere-ocean model for transient climate change, *Atmos. Ocean*, **33**, 683–730.
- Schmidt, G. A., et al. (2006), Present day atmospheric simulations using GISS ModelE: Comparison to in-situ, satellite and reanalysis data, *J. Clim.*, **19**, 153–192.

- Shindell, D. (2007), Local and remote contributions to Arctic warming, *Geophys. Res. Lett.*, **34**, L14704, doi:10.1029/2007GL030221.
- Shindell, D. T., and G. A. Schmidt (2004), Southern Hemisphere climate response to ozone changes and greenhouse gas increases, *Geophys. Res. Lett.*, **31**, L18209, doi:10.1029/2004GL020724.
- Shindell, D. T., G. Faluvegi, and N. Bell (2003), Preindustrial-to-present-day radiative forcing by tropospheric ozone from improved simulations with the GISS chemistry-climate GCM, *Atmos. Chem. Phys.*, **3**, 1675–1702.
- Shindell, D. T., B. P. Walter, and G. Faluvegi (2004), Impacts of climate change on methane emissions from wetlands, *Geophys. Res. Lett.*, **31**, L21202, doi:10.1029/2004GL021009.
- Shindell, D. T., G. Faluvegi, N. Bell, and G. A. Schmidt (2005), An emissions-based view of climate forcing by methane and tropospheric ozone, *Geophys. Res. Lett.*, **32**, L04803, doi:10.1029/2004GL021900.
- Shindell, D. T., G. Faluvegi, N. Unger, E. Aguilar, G. A. Schmidt, D. Koch, S. E. Bauer, and R. L. Miller (2006a), Simulations of preindustrial, present-day, and 2100 conditions in the NASA GISS composition and climate model G-PUCCINI, *Atmos. Chem. Phys.*, **6**, 4427–4459.
- Shindell, D. T., et al. (2006b), Multi-model simulations of carbon monoxide: Comparison with observations and projected near-future changes, *J. Geophys. Res.*, **111**, D19306, doi:10.1029/2006JD007100.
- Shine, K. P., T. K. Berntsen, and J. S. Fuglestad (2005), Scientific issues in the design of metrics for inclusion of oxides of nitrogen in global climate agreements, *Proc. Natl. Acad. Sci.*, **102**, 15,768–15,773.
- Stevenson, D. S., et al. (2006), Multi-model ensemble simulations of present-day and near-future tropospheric ozone, *J. Geophys. Res.*, **111**, D08301, doi:10.1029/2005JD006338.
- Streets, D., T. C. Bond, T. Lee, and C. Jang (2004), On the future of carbonaceous aerosol emissions, *J. Geophys. Res.*, **109**, D24212, doi:10.1029/2004JD004902.
- Sudo, K., M. Takahashi, and H. Akimoto (2003), Future changes in stratosphere-troposphere exchange and their impacts on future tropospheric ozone simulations, *Geophys. Res. Lett.*, **30**(24), 2256, doi:10.1029/2003GL018526.
- Unger, N., D. T. Shindell, D. M. Koch, M. Amann, J. Cofala, and D. G. Streets (2006), Influences of man-made emissions and climate changes on tropospheric ozone, methane and sulfate at 2030 from a broad range of possible futures, *J. Geophys. Res.*, **111**, D12313, doi:10.1029/2005JD006518.
- Van der Werf, G. R., J. T. Randerson, and G. J. Collatz (2003), Carbon emissions from fires in tropical and subtropical ecosystems, *Global Change Biol.*, **9**, 547–562.
- West, J. J., A. M. Fiore, L. W. Horowitz, and D. L. Mauzerall (2006), Global health benefits of mitigating ozone pollution with methane emission controls, *Proc. Natl. Acad. Sci.*, **103**, 3988–3993.
- Woodward, S., D. L. Roberts, and R. A. Betts (2005), A simulation of the effect of climate change-induced desertification on mineral dust aerosol, *Geophys. Res. Lett.*, **32**, L18810, doi:10.1029/2005GL023482.
- Zeng, G., and J. A. Pyle (2003), Changes in tropospheric ozone between 2000 and 2100 modeled in a chemistry-climate model, *Geophys. Res. Lett.*, **30**(7), 1392, doi:10.1029/2002GL016708.
- Ziemke, J. R., and S. Chandra (1999), Seasonal and interannual variabilities in tropical tropospheric ozone, *J. Geophys. Res.*, **104**, 21,425–21,442.
-
- S. E. Bauer, G. Faluvegi, D. M. Koch, R. L. Miller, G. A. Schmidt, and D. T. Shindell, NASA Goddard Institute for Space Studies, Center for Climate Systems Research, Columbia University, 2880 Broadway, New York, NY 10025, USA. (dshindell@giss.nasa.gov)
- S. Menon, Lawrence Berkeley Laboratory, Berkeley, CA, USA.
- R. L. Miller, Department of Applied Physics and Applied Mathematics, Columbia University, New York, NY, USA.
- D. G. Streets, Argonne National Laboratory, Argonne, IL, USA.
- N. Unger, Department of Atmospheric Sciences, University of Vermont, Burlington, VT, USA.